PHYSIOLOGY

Determinants of increased muscle insulin sensitivity of exercise-trained versus sedentary normal weight and overweight individuals

Dominik Pesta[1,2,3,4,5]†, Evrim Anadol-Schmitz[1,2]†, Theresia Sarabhai[6,1,2]†, Yvo Op den Kamp[7], Sofiya Gancheva[6,1,2], Nina Trinks[1,2], Oana-Patricia Zaharia[6,1,2], Lucia Mastrototaro[1,2], Kun Lyu[8], Ivo Habets[7], Yvonne M. H. Op den Kamp-Bruls[7], Bedair Dewidar[1,2], Jürgen Weiss[9,2], Vera Schrauwen-Hinderling[1,2,7], Dongyan Zhang[8], Rafael Calais Gaspar[8], Klaus Strassburger[2,10], Yuliya Kupriyanova[1,2], Hadi Al-Hasani[9,2], Julia Szendroedi[1,2,11], Patrick Schrauwen[1,12], Esther Phielix[7], Gerald I. Shulman[8,13], Michael Roden[6,1,2]*

The athlete's paradox states that intramyocellular triglyceride accumulation associates with insulin resistance in sedentary but not in endurance-trained humans. Underlying mechanisms and the role of muscle lipid distribution and composition on glucose metabolism remain unclear. We compared highly trained athletes (ATHL) with sedentary normal weight (LEAN) and overweight-to-obese (OVWE) male and female individuals. This observational study found that ATHL show higher insulin sensitivity, muscle mitochondrial content, and capacity, but lower activation of novel protein kinase C (nPKC) isoforms, despite higher diacylglycerol concentrations. Notably, sedentary but insulin sensitive OVWE feature lower plasma membrane-to-mitochondria *sn*-1,2-diacylglycerol ratios. In ATHL, calpain-2, which cleaves nPKC, negatively associates with PKCε activation and positively with insulin sensitivity along with higher GLUT4 and hexokinase II content. These findings contribute to explaining the athletes' paradox by demonstrating lower nPKC activation, increased calpain, and mitochondrial partitioning of bioactive diacylglycerols, the latter further identifying an obesity subtype with increased insulin sensitivity (NCT03314714).

INTRODUCTION

Surplus intramyocellular triglycerides (IMCT) are one of the strongest predictors of skeletal muscle insulin resistance in sedentary humans with or without obesity or type 2 diabetes and have been attributed to a mismatch between delivery and oxidation of fatty acids (*1*–*3*). Nevertheless, these triglycerides do not consistently relate to muscle insulin resistance (*4*) as endurance athletes (ATHL) maintain high insulin sensitivity despite a frequently observed elevation of IMCT (*5*, *6*). This conundrum has been termed the "athlete's paradox." Several mechanisms have been proposed to explain this conundrum, including improved mitochondrial oxidative capacity. However, although reduced mitochondrial oxidative capacity may contribute to lipid-induced insulin resistance by an imbalance between fatty acid delivery and oxidation (*7*–*10*), other studies reported a dissociation between muscle insulin sensitivity and oxidative capacity (*11*, *12*).

Insulin resistance is also associated with low-grade inflammation, which can be reduced by exercise training (*13*). Independent of total skeletal muscle lipid content, diacylglycerols (DAG), and ceramides have been reported as key mediators of insulin resistance in sedentary humans (*14*–*16*). In human skeletal muscle, increased *sn*-1,2-DAG stereoisomer content is associated with activation of the novel protein kinase C (nPKC) isoforms, PKCθ and PKCε, with subsequent inhibition of insulin signaling by serine-1101 phosphorylation of insulin receptor substrate 1 (*17*, *18*) and threonine-1160 phosphorylation of the insulin receptor, respectively (*12*, *15*). Ceramides have also been associated with muscle insulin resistance in humans (*16*, *19*) via decreasing insulin-stimulated protein kinase B (AKT) translocation (*20*).

One study reported the highest total muscle ceramide content in obese individuals but higher total muscle DAG in endurance-trained volunteers when compared to sedentary normal weight and obese humans (*21*). Recent studies, however, indicate that rather than total concentrations in skeletal muscle, the subcellular distribution of the stereoisomer, *sn*-1,2-DAG, is relevant for inducing insulin resistance in humans and animal models (*22*–*25*). Partitioning of DAG away from the plasma membrane into lipid droplets prevented nPKC activation in the liver and maintained hepatic insulin sensitivity in a murine model (*23*). Likewise, *sn*-1,2-DAG accumulation in the plasma membrane of livers of individuals with hepatic insulin resistance and metabolic dysfunction–associated steatotic liver disease was associated with nPKCε activation and inhibitory threonine-1160 phosphorylation of the insulin receptor kinase (*25*). Higher skeletal

[1]Institute for Clinical Diabetology, German Diabetes Center, Leibniz Center for Diabetes Research at Heinrich-Heine University, Düsseldorf, Germany. [2]German Center for Diabetes Research (DZD), Partner Düsseldorf, Düsseldorf, Germany. [3]Institute of Aerospace Medicine, German Aerospace Center (DLR), Cologne, Germany. [4]Centre for Endocrinology, Diabetes and Preventive Medicine (CEDP), University Hospital Cologne, Cologne, Germany. [5]Cologne Excellence Cluster on Cellular Stress Responses in Aging-Associated Diseases (CECAD), Cologne, Germany. [6]Department of Endocrinology and Diabetology, Medical Faculty and University Hospital, Heinrich-Heine University, Düsseldorf, Germany. [7]Department of Nutrition and Movement Sciences, School for Nutrition and Translational Research in Metabolism, Maastricht University, Maastricht, Netherlands. [8]Department of Internal Medicine, Yale School of Medicine, New Haven, CT, USA. [9]Institute for Clinical Biochemistry and Pathobiochemistry, German Diabetes Center, Leibniz Center for Diabetes Research at Heinrich-Heine University Düsseldorf, Medical Faculty, Düsseldorf, Germany. [10]Institute for Biometrics and Epidemiology, German Diabetes Center, Leibniz Center for Diabetes Research at Heinrich Heine University, Düsseldorf, Germany. [11]Department of Endocrinology, Diabetology and Clinical Chemistry (Internal Medicine 1), Heidelberg University Hospital, Heidelberg, Germany. [12]Leiden University Medical Center, Clinical Epidemiology, Leiden, Netherlands. [13]Department of Cellular and Molecular Physiology, Yale School of Medicine, New Haven, CT, USA.
*Corresponding author. Email: michael.roden@ddz.de
†These authors contributed equally to this work.

muscle *sn*-1,2-DAG ratios in the mitochondrial/endoplasmic reticulum fraction positively correlated with insulin sensitivity in humans (*24*). Muscle ceramide species have been associated with insulin resistance also in some (*16*, *24*) but not all studies (*18*, *26*, *27*). It still remains unclear, however, how endurance-trained individuals maintain high insulin sensitivity in light of potentially elevated intramyocellular DAG. By comprehensive phenotyping of individuals with a broad range of insulin sensitivity and physical fitness, we provide an alternative perspective on this long-standing question.

This observational study aimed at (i) comparing composition and subcellular localization of lipid mediators in different subcellular compartments and their possible association with insulin sensitivity in a cohort comprising endurance-trained ATHLs, sedentary healthy normal weight (LEAN), and overweight-to-obese (OVWE) individuals; (ii) thus assess alternative mechanisms to study the athlete's paradox; and (iii) explore the possible role of lipid mediators for subtyping individuals with obesity regarding the degree of insulin resistance.

RESULTS

ATHL with higher cardiorespiratory fitness have higher whole-body insulin sensitivity than untrained LEAN and OVWE humans

Of 116 enrolled, a total of 110 volunteers completed this study (fig. S1). ATHL and LEAN were of similar age, while OVWE were older than LEAN ($P < 0.01$; Table 1). Female representation was 36, 38, and 52% in OVWE, ATHL, and LEAN, respectively. As per group allocation, OVWE had highest BMI and also % body fat of all groups (both $P < 0.01$; Table 1). Hyperinsulinemic-euglycemic clamp tests revealed that whole-body insulin sensitivity (*M* value), mainly reflecting skeletal muscle insulin sensitivity (*28*), was 34 and 60% higher in ATHL than LEAN and OVWE, respectively (both $P < 0.01$; Table 1). Insulin-stimulated glucose oxidation and nonoxidative glucose disposal were higher in ATHL and LEAN compared to OVWE (all $P < 0.01$; Fig. 1A). The Δnonoxidative glucose disposal (NOXGD), i.e., the increase in glucose disposed but not oxidized under clamp conditions, was also higher in ATHL than in OVWE ($P < 0.01$; Fig. 1A). Respiratory exchange ratio (RER) was not different at baseline (0.83 ± 0.07 for ATHL, 0.83 ± 0.06 for OVWE, and 0.82 ± 0.07 for LEAN) but higher in ATHL than in OVWE (0.94 ± 0.07 versus 0.89 ± 0.06, $P = 0.003$) but not in LEAN (0.94 ± 0.06) during the clamp (Fig. 1B). The ΔRER, as a proxy of the so-called metabolic flexibility (*29*), was higher in ATHL and LEAN compared to OVWE ($P < 0.05$; Fig. 1C). Insulin-mediated suppression of endogenous glucose production (iEGP), reflecting hepatic insulin sensitivity, was higher in ATHL compared to OVWE ($P < 0.01$; Fig. 1D). As per preselection, maximal aerobic capacity (VO_2max) was higher in ATHL by 55% and by 40% compared to OVWE and LEAN, respectively (all $P < 0.01$; Table 1). Accounting for body composition differences, peak power output per lean mass was highest in ATHL, followed by LEAN and OVWE (all $P < 0.01$, Table 1). Fasting blood glucose and fasting plasma insulin were highest in OVWE (all $P < 0.01$ versus ATHL and LEAN; Table 1). None of the participants had diabetes according to current criteria (*30*). Fasting plasma triglycerides were lower in ATHL than in OVWE ($P < 0.01$), whereas fasting plasma non-esterified fatty acids (NEFAs) were higher in LEAN compared to ATHL ($P < 0.05$; Table 1). Of note, high-sensitivity C-reactive protein, a marker for systemic low-grade inflammation, was highest in OVWE compared to LEAN and ATHL ($P < 0.01$; Table 1).

ATHLs showed higher mitochondrial oxidative capacity and contacts with the lipid fraction as compared to OVWE humans

High-resolution respirometry was performed for ex vivo measurement of energy metabolism in biopsies of vastus lateralis muscle (*31*). Mitochondrial oxidative phosphorylation (OXPHOS) capacity, maximal respiratory capacity, i.e., oxygen consumption in the

Table 1. Participants characteristics of LEAN, OVWE, and ATHL. Data are means ± SD. Significant differences by one-way ANOVA denoted *$P < 0.05$, **$P < 0.01$, compared with LEAN; ^$P < 0.05$, ^^$P < 0.01$ compared with OVWE; ′$P < 0.05$, ″$P < 0.01$, compared with ATHL; hsCRP, high sensitivity C-reactive protein; OGIS, oral glucose insulin sensitivity index.

Parameter	LEAN ($n = 21$)	OVWE ($n = 55$)	ATHL ($n = 34$)
Age (years)	28 ± 4^^	35 ± 10**	30 ± 8
Sex (M/F)	10/11	35/20	21/13
Height (cm)	174.2 ± 7.7	175.0 ± 9.9	178.7 ± 7.6
Body mass (kg)	68 ± 7	98.8 ± 16.9	71.0 ± 8.7
BMI (kg/m^2)	22.4 ± 1.5^^	32.2 ± 4.8**,″	22.2 ± 1.5^^
Body fat (%)	27.0 ± 8.2^^	37.9 ± 9.1**,″	24.0 ± 9.2^^
VO_2max (ml kg^{-1} min^{-1})	33.9 ± 6.2^^,″	25.9 ± 5.6**,″	55.8 ± 7.4**,^^
Peak power output (W/kg lean mass)	3.9 ± 0.6^^,″	3.3 ± 0.6**,″	6.7 ± 0.5**,^^
Fasting blood glucose (mM)	4.4 ± 0.3^	4.7 ± 0.4*,″	4.4 ± 0.4^^
Fasting insulin (pM)	30.5 ± 17.4^^	77.1 ± 53.5**,″	25.0 ± 14.6^^
Fasting triglycerides (mM)	1.1 ± 0.5	1.6 ± 1.1**	0.8 ± 0.3^^
Fasting NEFAs (μM)	532 ± 229′	428 ± 183	380 ± 213*
Fasting hsCRP (nM)	10.5 ± 12.4^^	31.4 ± 34.3**,″	5.7 ± 5.7^^
M value (mg kg^{-1} min^{-1})	6.6 ± 2.1^^,″	4.0 ± 2.2**,″	9.9 ± 2.8**,^^
OGIS (ml/min per m^2)	468 ± 89^,″	405 ± 80*,″	546 ± 55**,^^

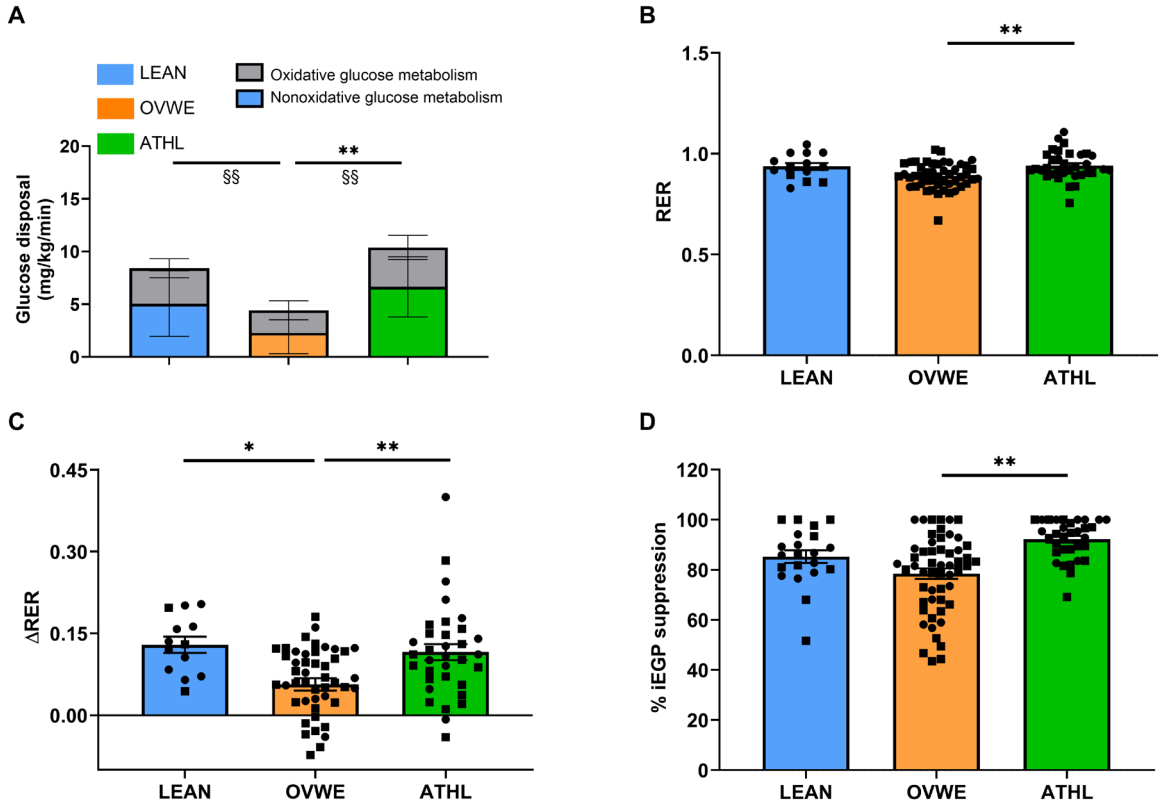

Fig. 1. Peripheral and hepatic insulin sensitivity, glucose oxidation, and metabolic flexibility. Oxidative and nonoxidative glucose disposal during insulin-stimulated conditions (**A**) and RER (**B**) during a hyperinsulinemic-euglycemic clamp as well as ΔRER from basal to clamped conditions as marker for metabolic flexibility (**C**); hepatic insulin sensitivity as iEGP (**D**). For (A), LEAN $n = 19$, OVWE $n = 51$, ATHL $n = 34$; for (B) and (C), LEAN $n = 14$, OVWE $n = 48$, ATHL $n = 34$; for (D), LEAN $n = 21$, OVWE $n = 54$, ATHL $n = 34$. Data are presented as means ± SEM; significant differences by one-way analysis of variance (ANOVA); $^*P < 0.05$, $^{**}P < 0.01$; for (A), ** compares oxidative glucose disposal and §§ nonoxidative glucose disposal; circles represent females and squares represent males; LEAN, normal weight, sedentary individuals; OVWE, overweight-to-obese; ATHL, athletes; RER, respiratory exchange ratio; iEGP, insulin-mediated suppression of endogenous glucose production.

noncoupled state at optimum uncoupler concentration, as well as fatty acid oxidation capacity per muscle wet weight, were highest in ATHL compared to the other groups (all $P < 0.01$; Fig. 2, A to C). The respiratory control ratio (RCR), as a proxy of mitochondrial coupling efficiency (*32*), as well as the leak control ratio (LCR), a proxy of mitochondrial proton leakage and coupling control (*33*), were not different between groups (fig. S2, A and B). Muscle citrate synthase activity (CSA), a surrogate marker of mitochondrial mass (*34*), was highest in ATHL compared to LEAN and OVWE (Fig. 2D). Likewise, mitochondrial (mt) DNA, another marker of mitochondrial content (*34*, *35*) was elevated in ATHL compared to LEAN and OVWE (fig. S2C). On the other hand, protein levels of peroxisome proliferator–activated receptor-gamma coactivator 1 alpha (PGC-1α), a key transcriptional regulator of mitochondrial biogenesis (*36*), were not different between groups (fig. S2D).

Using ^{1}H-magnetic resonance spectroscopy (MRS) for in vivo measurement of total IMCT in vastus lateralis muscle (*37*) revealed 32% higher IMCT content in ATHL and OVWE compared to LEAN (both $P < 0.01$; Fig. 3A), confirming the athlete's paradox. Likewise, in vitro transmission electron microscopy (TEM) performed in a representative subgroup (table S1) revealed higher lipid droplet volume density in ATHL than in LEAN ($P < 0.05$; Fig. 3B). More mitochondria had direct contact with lipid droplets (IMCT/mitochondrial juxtaposition) in ATHL than in OVWE ($P < 0.05$; Fig. 3C). Figure S3 shows examples of TEM images from all groups. Furthermore, type I fiber fraction was highest in ATHL, while type II fiber fraction (the fiber fraction not stained as type I fibers) of the vastus lateralis muscle was lowest in ATHL compared to the other groups (all $P < 0.01$; Fig. 3D).

ATHLs feature higher sequestration of DAG into the mitochondrial compartment

Using liquid chromatography tandem mass spectrometry (LC-MS/MS) methodology (*38*) revealed that *sn*-1,2-DAG accounted for ~64% of total DAG with the remainder consisting of about 15% of 2,3- and 20% of *sn*-1,3-DAG across all groups when summing up the five compartments. Purity of the subcellular fractions was assessed by Western blotting (fig. S4). Unexpectedly, ATHL had higher total *sn*-1,2-DAG, *sn*-1,3-DAG, and total DAG compared to OVWE and LEAN (all $P < 0.01$; Fig. 4A). Total ceramides were not different between groups (Fig. 4A). These comparisons were adjusted for age and sex.

Subcellular content of the various lipid species was analyzed in muscle samples upon fractionation by differential centrifugation (*38*). In the mitochondrial and endoplasmic reticulum compartment, *sn*-1,2-DAG were highest in ATHL compared to the other groups (all $P < 0.01$). Upon normalization to CSA, mitochondrial *sn*-1,2-DAG were higher in LEAN compared to ATHL ($P < 0.05$) but not different from OVWE. Cytosolic ($P < 0.01$) *sn*-1,2-DAG

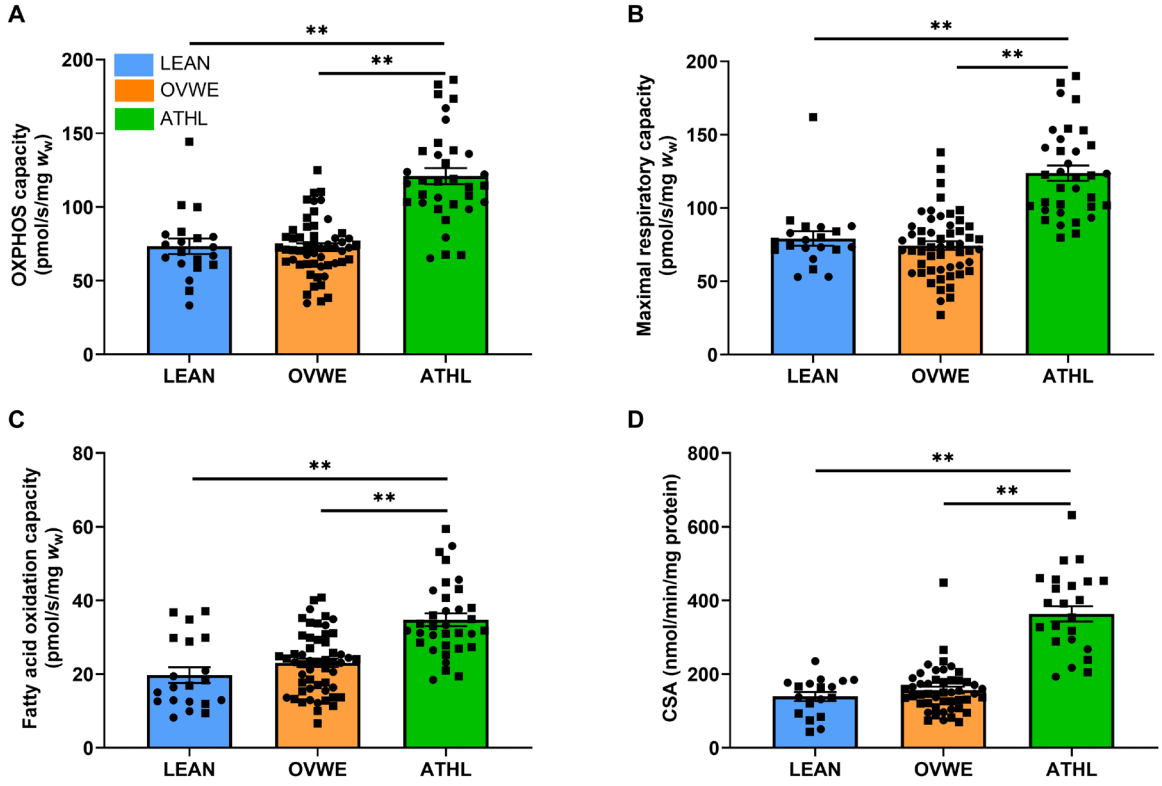

Fig. 2. Skeletal muscle mitochondrial function and content. In vitro OXPHOS capacity (**A**), maximal respiratory capacity (**B**), fatty acid oxidation capacity (**C**) assessed per wet weight (W_w) in permeabilized muscle fibers and expressed per W_w, and CSA (**D**). For (A) to (C), LEAN $n = 20$, OVWE $n = 54$, ATHL $n = 34$. For (D), LEAN $n = 18$, OVWE $n = 48$, ATHL $n = 27$. All muscle samples were obtained in the basal condition. Data are presented as means ± SEM; significant differences by one-way ANOVA; *$P < 0.05$, **$P < 0.01$; circles represent females, squares represent males.

were higher in ATHL when compared to OVWE, plasma membrane *sn*-1,2-DAG were higher in LEAN compared to OVWE ($P < 0.01$), while lipid-droplet *sn*-1,2-DAG were not different among the three groups (Fig. 4B). Of note, ATHL had also higher *sn*-1,3-DAG in the mitochondrial, endoplasmic reticulum, and cytosolic compartments compared to LEAN and OVWE (all $P < 0.05$) and higher *sn*-1,3-DAG in lipid droplets than LEAN ($P < 0.05$, fig. S5A). The intracellular distribution of *sn*-2,3-DAG was not different between groups (fig. S5B). Plasma membrane ceramides were lower in LEAN compared to OVWE ($P < 0.01$), and cytosolic ceramides were higher in ATHL compared to OVWE ($P < 0.05$) (fig. S5C).

Ratios of DAG between different intracellular compartments provide information on their subcellular distribution: ATHL and OVWE featured lower plasma membrane/mitochondrial *sn*-1,2-DAG than LEAN ($P < 0.01$; Fig. 4C), suggesting preferential shift of these lipids from plasma membrane toward mitochondrial compartments. Similar results were found for *sn*-1,3-DAG and *sn*-2,3-DAG ratios (Fig. 4C). Other ratios were not different among groups for *sn*-1,2-DAG, *sn*-1,3-DAG, and *sn*-2,3-DAG (fig. S5, D to F). All above comparisons were adjusted for age and sex.

Certain ratios of subcellular lipid species associate with parameters of insulin sensitivity

In the OVWE, *sn*-1,2-DAG ratios of plasma membrane/mitochondrial ($\beta = -0.28$; $P < 0.05$) associated with whole-body insulin sensitivity (Fig. 4D). This was also true for plasma membrane/lipid droplet ($\beta = -0.20$; $P < 0.05$), plasma membrane/cytosol ($\beta = -0.20$; $P < 0.05$), and plasma membrane/endoplasmic reticulum ($\beta = -0.27$; $P < 0.05$) ratios, which all associated negatively with whole-body insulin sensitivity (fig. S5, G and H) in OVWE. To further test the previously reported positive correlation of *sn*-1,2-DAG ratios in the mitochondrial/endoplasmic reticulum fraction with insulin sensitivity (*24*), we performed a subgroup analysis of OVWE group according to the upper 75th and lower 25th percentiles of the median of the plasma membrane/mitochondrial *sn*-1,2-DAG ratios. This allowed detecting phenotypic differences, with those exhibiting the lowest plasma membrane/mitochondrial *sn*-1,2-DAG ratios having higher whole-body insulin sensitivity, RCR and hexokinase II (HK II) protein content, but lower BMI, body fat content, and fasting NEFAs (Table 2). In addition, there was a trend ($P < 0.1$) toward higher physical fitness and lower PKCθ activation in this group. When using physical fitness (VO_2max) as the dependent variable, no associations were observed with DAG or ceramide species or their localization. Insulin sensitivity was positively associated with VO_2max only in the group with the highest *sn*-1,2-DAG ratio. Although cytosolic C16:0 and C18:0 ceramides have been associated with insulin resistance (*16*, *24*, *39*), we did not find these ceramide species to be different between the groups (Table 2).

ATHLs show an increase in skeletal muscle modulator proteases along with lower PKCθ activation but increased insulin signaling and intracellular glucose handling

PKCθ and PKCε are the predominant nPKC isoforms expressed in skeletal muscle. PKCθ translocation from cytosol to plasma membrane, reflecting its activation (*40*), was lower in ATHL than in

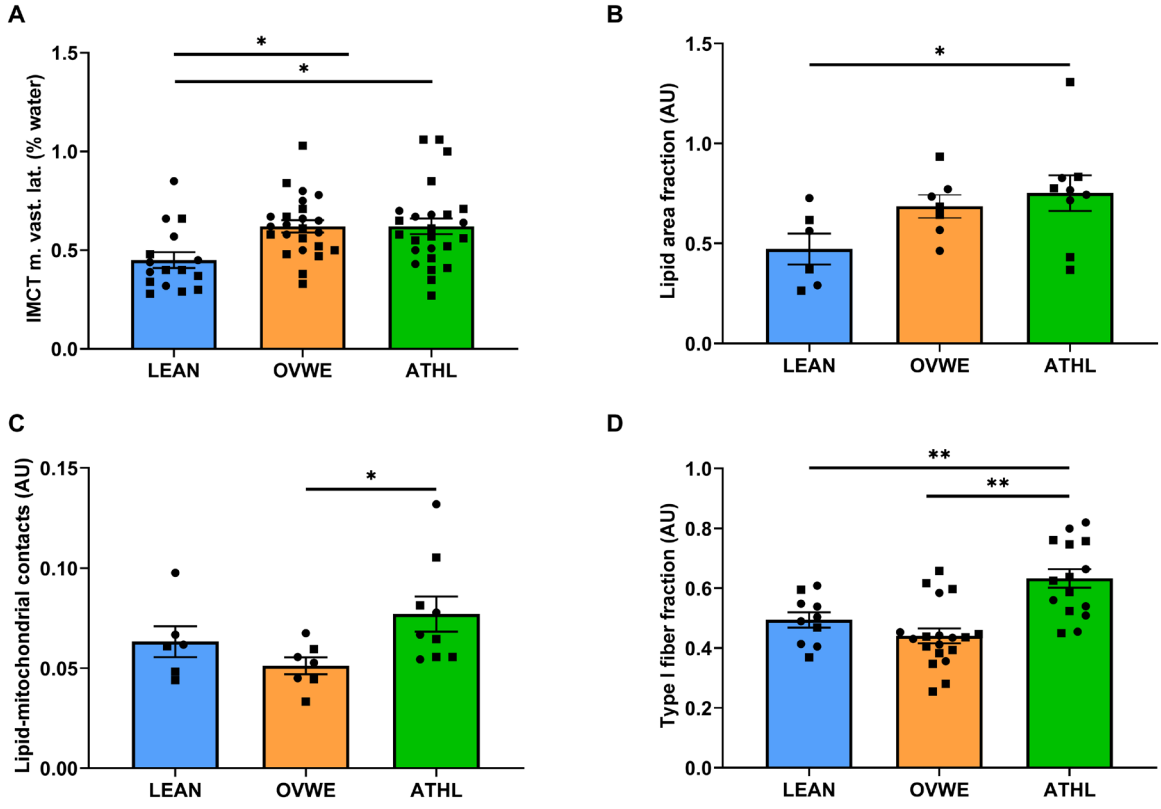

Fig. 3. Intramyocellular lipids and skeletal muscle morphology and fiber type. Intramyocellular lipids determined by ^{1}H-MRS (**A**) and lipid area fraction assessed by TEM from the vastus lateralis muscle (**B**) as well as contact sites between lipid droplets and mitochondria (**C**) and histologically determined skeletal muscle fraction of type 1 fibers in the vastus lateralis muscle (**D**). For (A), LEAN $n = 16$, OVWE $n = 24$, ATHL $n = 28$; for (B), LEAN $n = 6$, OVWE $n = 7$, ATHL $n = 9$; for (C) to (D), LEAN $n = 20$, OVWE $n = 54$, ATHL $n = 34$. All muscle samples were obtained in the basal condition. Data are presented as means ± SEM; significant differences by one-way ANOVA; $*P < 0.05$, $**P < 0.01$; circles represent females, squares represent males; IMCT, intramyocellular triglycerides; AU, arbitrary units.

OVWE ($P < 0.01$; Fig. 5A). There was also a trend for lower PKCε activation in ATHL compared to OVWE ($P = 0.08$; Fig. 5B). In ATHL, PKCε translocation was negatively associated with whole-body insulin sensitivity ($r = -0.61$, $P = 0.01$) and plasma membrane C18:0,C16:0 *sn*-2,3-DAG ($r = -0.62$, $P < 0.05$). In ATHL, PKCθ translocation correlated negatively with insulin sensitivity ($r = -0.42$, $P < 0.05$) (fig. S6, A to C).

The Ca^{2+}-dependent proteases, calpain 1 and calpain 2, can cleave nPKCs. Of note, calpain 2 was higher in both ATHL and LEAN (all $P < 0.05$; Fig. 5C) and calpain 1 tended to be higher in ATHL when compared to OVWE ($P = 0.08$) (fig. S7A). While insulin sensitivity correlated positively with calpain 1 ($r = 0.48$, $P = 0.007$) and calpain 2 ($r = 0.39$, $P = 0.03$) in ATHL, PKCε correlated negatively with calpain 2 ($r = -0.58$, $P = 0.02$). No such correlation was found in LEAN or OVWE (Fig. 5, D and E, and table S2). Serine-473 phosphorylation of AKT as a readout of distal insulin signal transduction was higher in ATHL than in both LEAN and OVWE (both $P < 0.05$; Fig. 5F). Protein expression of glucose transporter 4 (GLUT4) was higher in ATHL compared to OVWE and LEAN (both $P < 0.05$; Fig. 5G), while GLUT4 translocation as assessed from membrane-to-cytosol ratios was not different between groups. Protein content of HK II, the isoform regulated by insulin, was highest in ATHL and lower in both LEAN and OVWE ($P < 0.01$; Fig. 5H). The same was true for HK I, the other relevant isoform in human skeletal muscle (fig. S7B). In ATHL, HK II further correlated with whole-body insulin sensitivity ($r = 0.51$, $P = 0.04$). Images of the blots are available in the Supplementary materials (fig. S8).

Insulin resistance can be associated with activation of inflammatory pathways, specifically nuclear factor κ light-chain enhancer of activated B cells (NF-κB) (*41*). However, protein levels of muscle NF-κB and phosphorylated NF-κB did not differ between the groups (fig. S7, C and D).

Although this study was not designed to assess sex-specific differences, sex-based analyses for the main endpoints are provided in Table 3 and Fig. 6, A to H. Exploratory assessment of sex-specific differences revealed a higher percent body fat and lower maximal aerobic capacity in female participants. Further, high sensitivity C-reactive protein (hsCRP) was higher in female compared to male OVWE, and whole-body insulin sensitivity was lower in female compared to male ATHL (Table 3). There were no other differences for other outcomes of this study (Fig. 6, A to H).

DISCUSSION

This observational study demonstrates that the ATHL's higher insulin sensitivity, despite their greater IMCT content, associates with lower nPKCθ activation. Lower nPKC activation may result from preferential partitioning of bioactive DAG to the mitochondria relative to other subcellular compartments but also from the observed increased intracellular calpain proteases, which can cleave nPKC

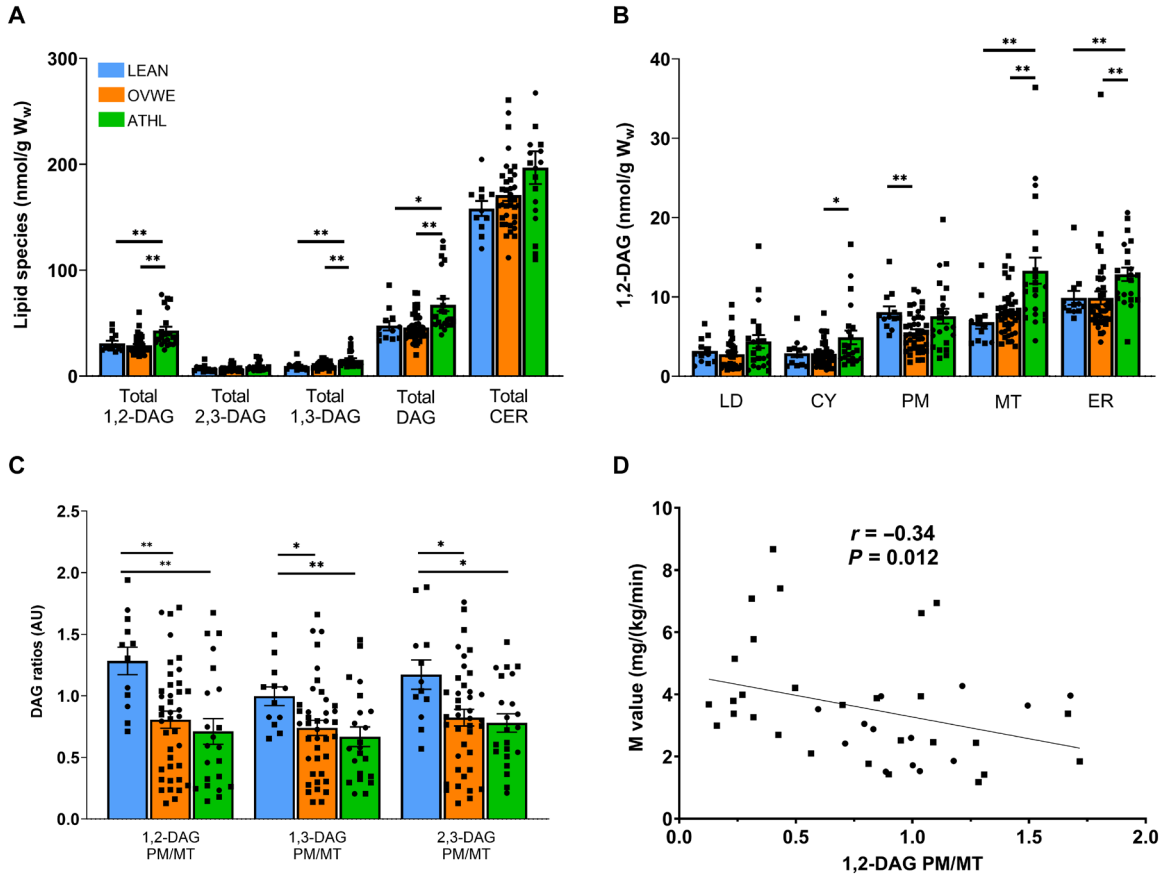

Fig. 4. Concentration of DAG and ceramides in five fractions (lipid droplet, cytosol, plasma membrane, mitochondria, and endoplasmic reticulum) in skeletal muscle. Concentration of *sn*-1,2-DAG, *sn*-2,3-DAG, *sn*-1,3-DAG, total DAG, and total ceramides (**A**); *sn*-1,2-DAG concentration in either lipid droplet (LD), cytosolic (CY), plasma membrane (PM), mitochondrial (MT), or endoplasmic reticulum (ER) subcellular compartments (**B**); ratios in subcellular compartments of PM to MT *sn*-1,2-DAG, *sn*-1,3-DAG, and *sn*-2,3-DAG (**C**); association of whole-body insulin sensitivity (*M*-value) with plasma membrane/mitochondrial ratios of *sn*-1,2-DAG for the OVWE group (**D**). For (A) to (C), LEAN $n = 12$, OVWE $n = 40$, ATHL $n = 22$; for (D), $n = 41$. All muscle samples were obtained in the basal condition. Data are presented as means ± SEM or Pearson correlations; significant differences by one-way ANOVA; $^{*}P < 0.05$, $^{**}P < 0.01$; circles represent females; squares represent males.

despite the presence of DAG in the plasma membrane and positively relate to insulin sensitivity and negatively to nPKC activation. Further, the highly regulated metabolic environment in ATHLs' myocytes such as higher oxidative metabolism per se and greater protein abundance of myocellular GLUT4 and HK II likely contribute to the higher insulin sensitivity of athletes, independent of increased lipid availability (*42*). Moreover, lower plasma membrane/mitochondrial 1,2-DAG ratio identifies a subtype of overweight/obesity with higher insulin sensitivity, which may help for precision medicine in obesity and further underlines relative distribution of DAG within intracellular compartments instead of absolute cellular levels of DAG.

We compared baseline data of three groups composing of individuals covering a wide range of insulin sensitivity and physical fitness. We carefully selected these groups, which can be discriminated not only by their maximal aerobic capacity but also by their peak power output normalized to lean mass. OVWE showed notable impairments of skeletal muscle and hepatic insulin sensitivity (*43*, *44*). The majority of the whole body-insulin resistance of OVWE could be attributed to an ~60% reduction in insulin-stimulated nonoxidative glucose disposal and to a minor extent to a decrease in glucose oxidation. In contrast, ATHLs can maintain elevated nonoxidative capacity for muscle glycogen synthesis even under conditions of excessive lipid availability, e.g., by intravenous lipid infusion (*45*). Key components of the insulin signaling cascade and glucose uptake pathway were up-regulated in skeletal muscle of ATHL as compared to OVWL and LEAN. The increase in serine-473 phosphorylation of AKT is in line with observations upon acute or short-term exercise and long-term endurance training in humans (*46*, *47*), while lower serine-473 phosphorylation of AKT has been frequently described in adipose tissue and skeletal muscle of insulin-resistant states like type 2 diabetes and obesity (*48*–*50*).

Using two independent methods, this study confirms the previously reported higher IMCL for both ATHL and OVWE than in LEAN (*5*, *21*, *51*, *52*). The simultaneous absence of insulin resistance in ATHL underlines that cellular neutral lipid content or absolute cellular levels of DAG are not primarily responsible for inhibiting insulin signaling. Impaired mitochondrial oxidative capacity likely plays a key role for regulating ectopic lipid deposition, bioactive lipid metabolites, and organ-specific insulin resistance, as diminished mitochondrial fatty acid oxidative capacity can favor intracellular buildup of bioactive lipid metabolites and adversely affect

Table 2. Subgroups of OVWE with lowest and highest plasma membrane/mitochondrial *sn*-1,2-DAG ratios. Data are means ± SD. Significant differences by unpaired *t* test denoted *$P < 0.05$, **$P < 0.01$, compared with highest 1,2-DAG PM/MT.

Parameter	Lowest 1,2-DAG PM/MT ($n = 15$)	Highest 1,2-DAG PM/MT ($n = 15$)
Age (years)	35 ± 7	38 ± 11
Sex (M/F)	14/1	9/6
BMI (kg/m^2)	30.6 ± 4.1	35.1 ± 3.9**
Body fat (%)	30.7 ± 4.3	40.8 ± 8.0**
VO_2max (ml min^{-1} kg^{-1})	28.3 ± 9.9	24.0 ± 5.2
M value (mg min^{-1} kg^{-1})	4.5 ± 1.8	3.1 ± 1.7*
Fasting blood glucose (mM)	4.9 ± 0.6	4.7 ± 0.4
HbA1c (%) [mmol/mol]	5.1 ± 0.4 [32 ± 4.4]	5.2 ± 0.3 [33 ± 3.3]
Fasting insulin (pM)	64.6 ± 36.8	86.1 ± 52.9
Fasting hsCRP (nM)	19.0 ± 19.0	38.1 ± 28.6
Fasting NEFAs (μM)	309.3 ± 91.2	557.3 ± 154.5**
iEGP suppression (%)	76.1 ± 13.1	72.2 ± 19.8
FIB-4 (AU)	0.63 ± 0.19	0.65 ± 0.16
OXPHOS capacity (pmol s^{-1} mg^{-1})	69.0 ± 16.8	74.2 ± 23.6
Fatty acid oxidation capacity (pmol s^{-1} mg^{-1})	24.7 ± 10.5	23.8 ± 7.5
CSA (nmol min^{-1} mg^{-1} protein)	141.3 ± 48.4	169.8 ± 91.3
RCR	4.1 ± 1.0	2.6 ± 0.9**
GLUT4 protein content (AU)	1.3 ± 0.7	1.2 ± 0.3
HK II protein content (AU)	0.9 ± 0.4	0.4 ± 0.3*
Calpain 1 protein content (AU)	0.9 ± 0.3	0.8 ± 0.3
Calpain 2 protein content (AU)	0.7 ± 0.4	0.7 ± 0.3
PKCθ translocation (M/C ratio)	1.9 ± 0.9	3.9 ± 1.8
Total cytosolic ceramides (nmol/g)	31.3 ± 7.8	31.7 ± 5.0
Cytosolic C16:0 ceramides (nmol/g)	0.02 ± 0.01	0.02 ± 0.01
Cytosolic C18:0 ceramides (nmol/g)	0.06 ± 0.02	0.06 ± 0.02

glucose homeostasis (*12*, *53*). In this context, lipid droplets and mitochondria form a functional organelle pair to maintain cellular energy homeostasis, also during exercise training, serving to improve mitochondrial fatty acid oxidation (*54*). ATHL showed more lipid-mitochondrial contact sites than OVWE, as reported for myocytes of active and athletic populations (*55*), along with greater fatty acid–oxidative capacity. Higher exercise-induced utilization of intramyocellular lipids may therefore protect against DAG-induced insulin resistance in physically active individuals (*42*, *56*, *57*). Both longitudinal training studies (*58*) as well as cross-sectional studies (*59*) also indicate a shift toward type I fibers or a more oxidative phenotype after endurance training. As type II fibers have generally lower oxidative capacity and enzyme activity, the distinct prevailing fiber type profile of our cohorts potentially relates to their metabolic phenotype (*60*). Of note, the immune histology approach did not allow to further distinguish between type IIa and IIx fibers. It still remains largely unclear, however, whether endurance-trained ATHLs simply have more mitochondria or whether intrinsic mitochondrial differences set these individuals apart from their untrained counterparts. We find that both CSA and mtDNA, two established markers for mitochondrial content, to be highest in the ATHL group, which aligns with existing literature (*61*–*63*). Here, we show that mitochondrial coupling efficiency, as determined from RCRs and LCRs, was comparable, indicating that this parameter is not related to energetic capacity. These findings align with previous observations made in trained and untrained individuals (*64*). In the present study, PGC-1α expression reflecting mitochondrial biogenesis was not increased in ATHL, which might be due to the timing of the muscle biopsy at least 48 hours after the last exercise bout. While rapidly up-regulated after acute exercising (*65*), PGC-1α transcript levels remain elevated for only about 24 hours and decline substantially after 48 hours (*66*). Nevertheless, the present comprehensive study underlines the concept of quantitative rather than qualitative mitochondrial adaptations to endurance training.

The similarly higher IMCT in both ATHL and OVWE draws the attention to subcellular localization and distribution of bioactive lipids to explain the difference in insulin sensitivity between these groups. Several studies identified higher membrane DAG (*18*, *67*) but lower (*67*), similar (*68*), or higher (*18*) cytosolic DAG to be associated with acute experimental or chronic common insulin resistance. The present study used advanced protocols now allowing for separation of five instead of only two subcellular compartments (*25*). Previously only used in liver samples to elucidate the connection of hepatic plasma membrane DAG species and hepatic insulin resistance via activating PKCε (*25*), this technique has now been adapted for skeletal muscle tissue (*69*). Of note, the "membrane" fraction used in earlier

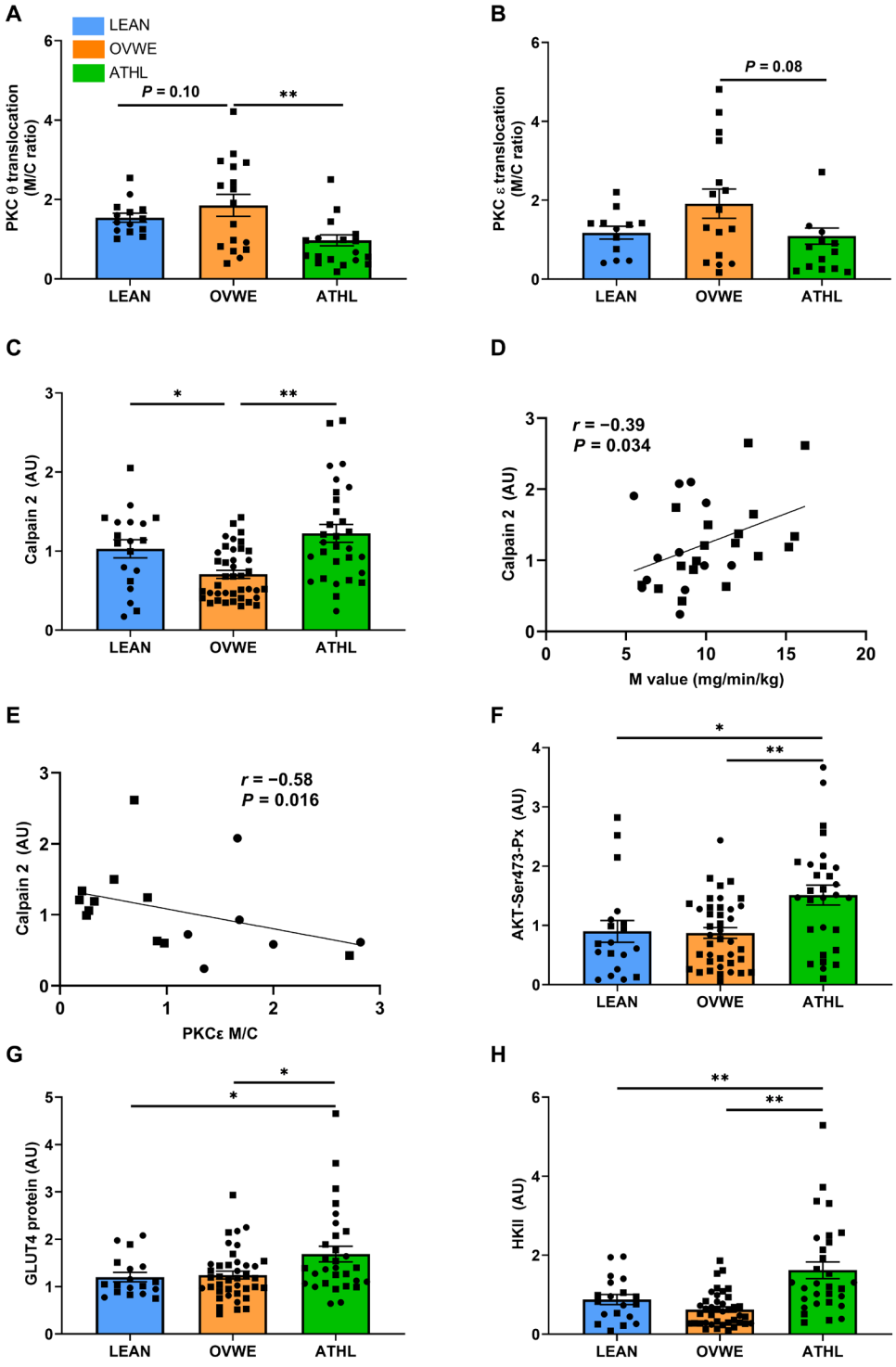

Fig. 5. Increased myocellular insulin signaling and intracellular glucose handling as well as elevated modulator proteases elucidate the clinical phenotype. PKCθ (**A**) and PKCε (**B**) translocation derived from the membrane-to-cytosol ratio, calpain 2 (**C**), association of calpain 2 with *M* value (**D**) as well as calpain 2 with PKCε for the ATHL group (**E**), serine-473 phosphorylation of AKT (**F**), total GLUT4 protein (**G**), and HK II protein (**H**). For (A) and (B), LEAN $n = 14$, OVWE $n = 17$, ATHL $n = 23$; for (C), LEAN $n = 19$, OVWE $n = 40$, ATHL $n = 30$; for (D), $n = 30$; for (E), $n = 17$; for (F) to (H), LEAN $n = 18$, OVWE $n = 40$, ATHL $n = 30$. For (A), (B), and (G), muscle samples were obtained in the basal condition; for (C), (F), and (H), muscle samples were obtained during insulin-stimulated conditions. Data are presented as means ± SEM; significant differences by one-way ANOVA; $^{*}P < 0.05$, $^{**}P < 0.01$; GLUT, glucose transporter; Ser-Px-serine phosphorylation; circles represent females and squares represent males.

Table 3. Participants' characteristics and main outcomes of LEAN, OVWE, and ATHL, stratified according to sex. Data are means ± SD. Significant differences by one-way ANOVA denoted $^{*}P < 0.05$, $^{**}P < 0.01$, compared with LEAN female; $^{\wedge}P < 0.05$, $^{\wedge\wedge}P < 0.01$ compared with OVWE female; $^{\prime}P < 0.05$, $^{\prime\prime}P < 0.01$, compared with ATHL female; $^{@}P < 0.05$, $^{@@}P < 0.01$, compared with LEAN male, $^{\#}P < 0.05$, $^{\#\#}P < 0.01$ compared with OVWE male, $^{\S}P < 0.05$, $^{\S\S}P < 0.01$, compared with ATHL male.

Parameter	LEAN female ($n = 11$)	LEAN male ($n = 10$)	OVWE female ($n = 20$)	OVWE male ($n = 35$)	ATHL female ($n = 13$)	ATHL male ($n = 21$)
Age (years)	29 ± 6	29 ± 4	34 ± 6	39 ± 12	29 ± 6	32 ± 10
BMI (kg/m^2)	21.7 ± 2.1	22.3 ± 1.2	35.6 ± 4.0	32.2 ± 4.8	22.0 ± 1.2	22.6 ± 1.6
Body fat (%)	32.5 ± 10.6@@	21.9 ± 5.2**	47.1 ± 6.3$^{\#\#}$	33.9 ± 5.8^^	28.0 ± 4.4§	21.4 ± 3.8′
VO_2max (ml kg^{-1} min^{-1})	27.1 ± 2.3@@	38.6 ± 5.5**	22.0 ± 4.2$^{\#}$	27.0 ± 5.0^	48.4 ± 4.0§§	58.9 ± 5.4″
Fasting blood glucose (mM)	4.5 ± 0.2	4.4 ± 0.3	4.6 ± 0.0.3	4.9 ± 0.5	4.3 ± 0.3	4.4 ± 0.4
Fasting insulin (pM)	37.5 ± 34.3	20.1 ± 12.5	69.4 ± 80.5	43.8 ± 57.6	21.5 ± 27.1	10.4 ± 16.7
Fasting triglycerides (mM)	0.86 ± 0.30	1.29 ± 0.62	1.35 ± 0.89	1.77 ± 1.19	0.89 ± 0.39	0.73 ± 0.22
Fasting NEFAs (μM)	601.3 ± 232.1	468.0 ± 216.3	478.9 ± 186.2	397.4 ± 176.1	450.8 ± 238.6	339.3 ± 191.9
Fasting hsCRP (nM)	33.3 ± 14.3	8.6 ± 9.5	52.4 ± 49.5$^{\#\#}$	20.0 ± 12.4^^	5.7 ± 4.8	5.7 ± 7.6
M value (mg kg^{-1} min^{-1})	5.6 ± 0.6	8.3 ± 1.6	2.8 ± 1.0	3.8 ± 2.0	7.7 ± 1.9§§	11.5 ± 2.7″
OGIS (ml/min per m^2)	454.0 ± 89.9	498.5 ± 82.2	428.2 ± 57.1	391.6 ± 88.9	538.9 ± 57.7	549.5 ± 55.5

studies consists of plasma, mitochondrial, endoplasmic reticulum, Golgi, and other endomembranes, rendering interrogations of precise DAG compartmentation difficult (*23*). By using this advanced approach (*69*), the present study showed that bioactive *sn*-1,2-DAG species are preferentially sequestered into the mitochondrial compartment in skeletal muscle of ATHL. These differences in DAG concentration likely arise from increased mitochondrial content in ATHL. The reason for the preferential sequestration into the mitochondrial compartment goes beyond the scope of this study and warrants further investigation in future studies. Lower ratios of plasma membrane/mitochondrial *sn*-1,2-DAG in ATHL support the concept of relative distribution of DAG within intracellular compartments that is metabolically significant, whereas the higher total DAG likely provide increased substrates for fatty acid oxidation. Accordingly, fatty acid oxidation was increased in ATHL. Likewise, subanalysis of the OVWE group uncovered that sedentary OVWE individuals with the lowest *sn*-1,2-DAG ratios in the plasma membrane/mitochondrial compartment also show advantageous metabolic characteristics including better insulin sensitivity, body composition, lipid metabolism, and mitochondrial coupling control. Although the sex distribution is skewed toward males in the low *sn*-1,2-DAG ratio group, it is unlikely that this affects the conclusions, as the exploratory analysis revealed no sex-specific differences with regard to this outcome. When setting physical fitness (VO_2max) as the dependent variable, no associations were found for DAG and ceramide species and localization. Insulin sensitivity was only positively associated with VO_2max in the highest *sn*-1,2-DAG ratio group. A compilation of these traits likely contributes to an improved metabolic phenotype seen in this subgroup. These results are building on earlier findings of subtypes of individuals with diabetes and prediabetes (*70*, *71*). The phenotypic signature of the subtypes of type 2 diabetes comprises those with severe insulin-deficient diabetes, severe insulin-resistant diabetes, mild obesity-related diabetes, and mild age-related diabetes, which differ in the degree of insulin resistance and cardiometabolic risk factors (*70*, *71*). Cytosolic C16:0 and C18:0 ceramides, previously being associated with insulin resistance (*16*, *24*, *39*), were not different in our subgroups. In conclusion, partitioning of bioactive lipids away from the plasma membrane into the mitochondrial compartment associates with features of higher insulin sensitivity.

The present study reports higher activation of PKCθ and PKCε in OVWE than in the other groups. As the DAG-nPKC pathway may not fully explain the athlete's paradox, we examined innovative alternative mechanisms, particularly the role of the intracellular modulator proteases, calpain 1 (μ-calpain) and 2 (m-calpain). The cysteine proteases, calpain 1 and calpain 2, are involved in Ca^{2+}-dependent remodeling of myocellular proteins (*72*) but also in degrading different PKC isoforms (*73*). The conventional isoform, PKCα, colocalizes with calpain 1 in the membrane of rabbit skeletal muscle (*74*) and calpain inhibition by antisense oligonucleotides increases PKCδ concentrations in cultured myoblasts (*75*). The key finding that calpain cleaves PKC subspecies in the presence of phospholipids and DAG (*76*) suggests that DAG-activated PKCs are preferentially targeted for proteolysis and may help to explain the lower PKCθ translocation despite higher DAG in ATHL of the present study. The increase in calpain may result from augmented sarcoplasmic Ca^{2+} release in myocytes, as reported for chronic endurance training (*77*), which would activate the Ca^{2+}-dependent calpain. The positive association of calpain 2 with insulin sensitivity and its negative association with nPKC activation in ATHL support this concept. These findings provide an insightful mechanistic advancement for how chronic exercise training potentially prevents activation of PKCs by recruiting modulator proteases to remodel the intracellular environment.

In the muscle, C18 ceramides have previously been associated with insulin resistance (*16*, *24*), but the present study did not detect any association of ceramides with insulin resistance. The absence of

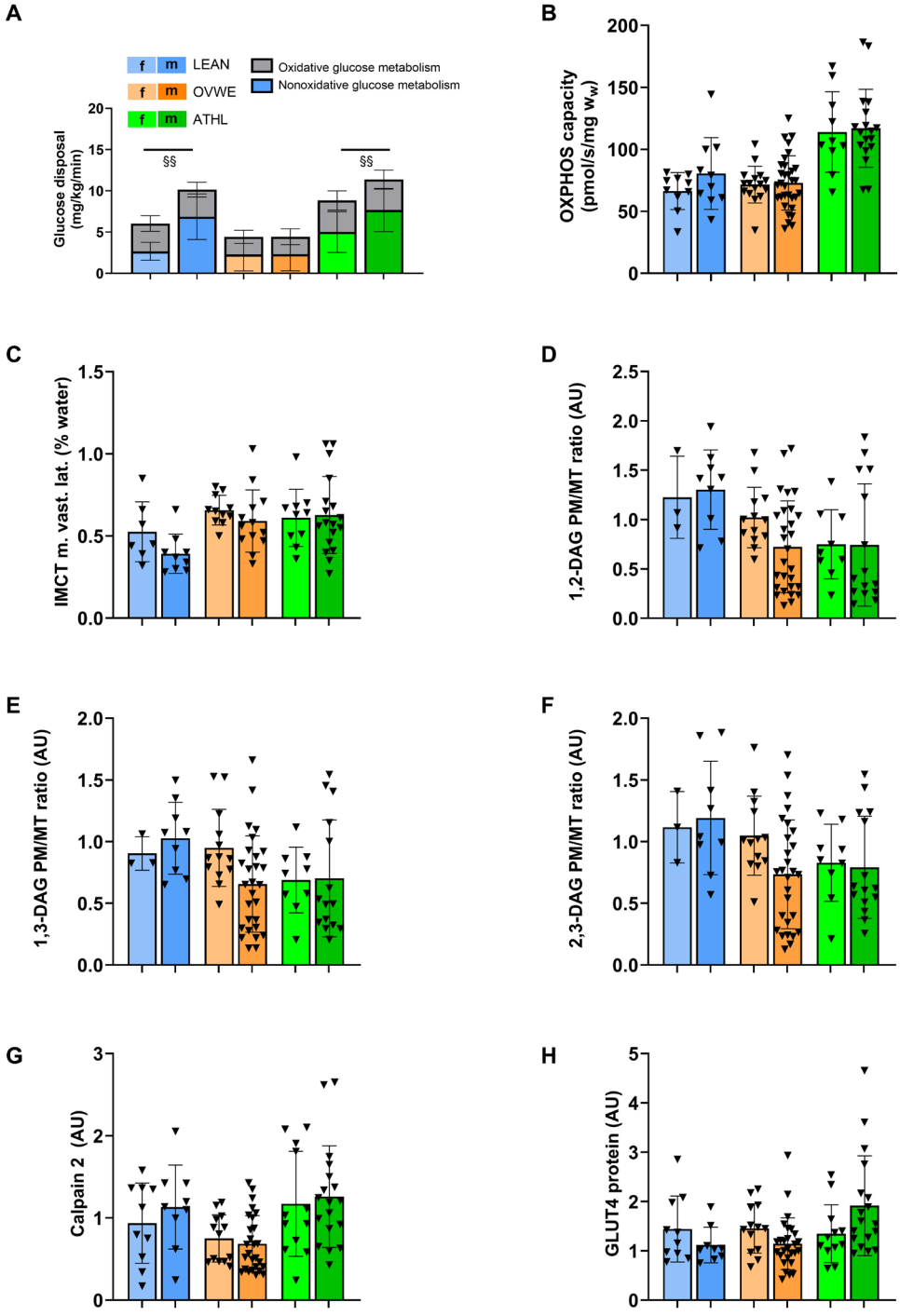

Fig. 6. Sex-specific comparison of glucose disposal, mitochondrial function, intramyocellular lipids, calpain 2, and GLUT4 protein content. Oxidative and non-oxidative glucose disposal during insulin-stimulated conditions (**A**); in vitro mitochondrial OXPHOS capacity (**B**); intramyocellular lipids determined by ^{1}H-MRS (**C**); ratios in subcellular compartments of PM-to-MT *sn*-1,2-DAG (**D**), *sn*-1,3-DAG (**E**), and *sn*-2,3-DAG (**F**), calpain 2 (**G**), and total GLUT4 protein content (**H**). For (A), LEAN f $n = 9$, LEAN m $n = 12$; OVWE f $n = 19$; OVWE m $n = 32$; ATHL f $n = 13$; ATHL m $n = 21$. For (B), LEAN f $n = 10$; LEAN m $n = 10$; OVWE f $n = 16$; OVWE m $n = 32$; ATHL f $n = 10$; ATHL m $n = 18$. For (C), LEAN f $n = 7$; LEAN m $n = 9$; OVWE f $n = 11$; OVWE m $n = 13$; ATHL f $n = 10$; ATHL m $n = 18$. For (D) to (F), LEAN f $n = 3$; LEAN m $n = 9$; OVWE f $n = 13$; OVWE m $n = 28$; ATHL f $n = 9$; ATHL m $n = 15$. For (G) and (H), LEAN f $n = 10$; LEAN m $n = 9$; OVWE f $n = 13$; OVWE m $n = 27$; ATHL f $n = 12$; ATHL m $n = 18$. All muscle samples were obtained in the basal condition. Data are presented as means ± SEM; significant differences by one-way ANOVA; §§$P < 0.01$ for nonoxidative glucose disposal; f, female; m, male; DAG, diacylglycerol.

a relationship of this putative mediator of insulin resistance is in line with other studies in healthy lean persons, insulin-resistant obese individuals, and obese humans with type 2 diabetes (*78*). This is in contrast to other findings reporting an association of ceramides and other sphingolipids, in particular, muscle C18 ceramides, with insulin resistance (*16*, *24*). These divergent findings may be related to the fact that samples were not fractionated (*16*) or assayed in different subcellular fractions (*24*). Of note, activation of inflammatory pathways such as NF-κB, which have been related to ceramide-mediated insulin resistance (*79*), was also not found in the present study. Nevertheless, the relevance of the NF-κB pathway in mediating obesity-induced insulin resistance remains a matter of debate (*80*).

Here, ATHL featured higher muscle GLUT4 content, likely reflecting their higher cellular glucose transport. Glucose transport activity has been established as the rate-controlling step in insulin-stimulated muscle glycogen synthesis in humans (*81*). ATHL generally feature higher abundance of GLUT4 protein than sedentary individuals (*82*). In the present study, ATHL also showed higher muscle HK II content, which positively associated with whole-body insulin sensitivity. Increased HK II activity indicates improved glucose phosphorylation capacity, which allows for higher muscle glucose disposal (*45*) and also contributes to control of glycogen synthetic rates (*81*). In this context, bed rest–induced insulin resistance has been related to lower amounts of the muscle proteins involving glucose transport, phosphorylation, and storage, including GLUT4 and HK II levels (*83*). The above studies, along with the role of HK II protein for exercise endurance (*84*), may help to explain the operation of multiple mechanisms underlying the higher insulin sensitivity of ATHL aside from changes in cellular lipid distribution.

Some limitations of this study require attention. The relatively large cohort size for a study aiming at comprehensive phenotyping still may not account for the inherent biological variability, as reflected by the rather small effect sizes, which may also limit the generalizability of within-group correlations. In addition, this study was not designed and powered to assess sex-specific differences; an exploratory sex-based analysis of the main study outcomes revealed higher body fat content and lower aerobic capacity in females than in males, a higher hsCRP in female than in male OVWE, and lower whole-body insulin sensitivity in female than in male ATHL, whereas the remainder of metabolic outcomes did not reveal sex-specific differences. Further, despite the slightly younger age of the LEAN than the OVWE group, the differences in features of glucose metabolism cannot be explained by this age difference as age-adjusted statistical analyses are negligible. This confirms previous analyses, which also found no age-related differences in glucose tolerance between young and middle-aged cohorts (*85*). Of note, this cross-sectional study in humans does not allow to derive direct causal relationships. Moreover, the relatively small amount of available muscle tissue has limited the analyses to the main aims of the study, e.g., myocellular acylcarnitine concentrations, also associated with lipid-mediated insulin resistance by some (*86*), but not others (*78*), were not measured in the present study. Last, limitations in fractionation quality apply as human biopsy samples cannot undergo in situ freeze-clamping due to ethical and safety reasons, which would likely enable cleaner compartment isolation. In addition, limited tissue availability prevented further validation across additional markers in all participants.

In conclusion, this observational study provides alternative explanations of the athlete's paradox by demonstrating that higher insulin sensitivity in ATHL tightly associates with relative distribution of DAG within intracellular compartments toward the mitochondrial compartment and by skeletal muscle calpain, which contributes to lower nPKC activation despite increased absolute myocellular lipid content. Further analyses allowed to identify a subgroup of highly insulin-sensitive overweight/obese people with lower plasma membrane/mitochondrial ratio of *sn*-1,2-DAG, which also feature lower cardiometabolic risk factors and could thereby contribute to precision medicine in obesity.

MATERIALS AND METHODS

Study participants

Participants aged 18 to 69 years were recruited via social media or advertisements in local newspapers between April 2017 and January 2023 for this observational study reporting baseline data and not reporting any result of an interventional clinical trial. A total of 165 individuals were assessed for eligibility, of whom 49 were excluded because of not meeting the inclusion criteria. The remaining 116 individuals were enrolled in this observational study and received compensation for taking part in the study. After enrollment, six individuals were excluded, of whom five declined to further participate and one due to pregnancy (see STROBE Diagram fig. S1). After obtaining informed consent, a total of 110 individuals comprising young male and female LEAN ($n = 21$) individuals (BMI < 25), OVWE ($n = 55$) individuals (BMI > 25), and endurance-trained ATHLs participating in cycling, running, or triathlon events (ATHL, $n = 34$) were included in the present study. OVWE and ATHL were matched by IMCT levels obtained via ^{1}H-MRS. They consented to the trial protocol (ClinicalTrials.gov registration no. NCT03314714), which was approved by the ethics board of Heinrich-Heine University Düsseldorf (ref. number 5722R) as well as the ethics board of Maastricht University Medical Center (Medical Ethics Review Committee ref. number 173021) and carried out in accordance with the current (2013) version of the Declaration of Helsinki. Inclusion criteria for ATHL were VO_2max ≥ 60 ml kg^{-1} min^{-1} ♂ and ≥ 45 ml kg^{-1} min^{-1} ♀, while LEAN and OVWE were inactive (structured exercising <1 hour/week) healthy individuals with VO_2max < 40 ml kg^{-1} min^{-1}. Exclusion criteria for all participants were smoking; acute or chronic diseases including cancer, diabetes or prediabetes, and kidney and cardiovascular diseases; or pregnancy. None of the participants were taking medications, and the participants were weight stable throughout the study. The participants were examined on two nonconsecutive days within 2 weeks. Body weight was measured during screening and before the clamp test to ensure stability. Weight stability was also confirmed via self-report during the initial phone interview and before study inclusion, with only those reporting stable weight in the preceding 6 months being included.

Study design

This observational, noninterventional study focused on analysis of baseline metabolic parameters. From the three parts of original study protocol, we performed only the first observational subproject and report its baseline results here. This study does not report any result of an interventional clinical trial. The primary objectives of this study were to assess insulin sensitivity and its association to intramyocellular lipid content in three groups with different degrees of insulin sensitivity and physical fitness. The examinations were carried out at the German Diabetes Center, Düsseldorf, Germany,

and at the Maastricht University Medical Center, Maastricht, The Netherlands. All volunteers underwent screening including medical history, clinical examination, 12-lead electrocardiogram, and anthropometric measurements including height and weight and routine laboratory analyses (see below). Persons with elevated routine laboratory parameters (>twofold upper reference values) were excluded. All participants underwent a 75-g oral glucose tolerance test (OGTT) to exclude dysglycemia (*30*). Three individuals of the OVWE group presented with impaired glucose tolerance (2-hour glucose concentration during the OGTT >140 mg/dl). All participants performed an incremental exhaustive exercise test on a cycle ergometer (Viasprint 200, Ergoline, Bitz, Germany) to obtain their VO_2max, and exhaustion was defined according to the guidelines on cardiopulmonary exercise testing (*87*).

Upon inclusion, all participants were examined on two nonconsecutive days within a 2-week period after an overnight fast and ATHL abstained from exercise training for at least 48 hours before the examinations. On the first day, ^{1}H-MRS of the m. vastus lateralis of the left leg was performed in the fasted state, followed by bioimpedance analysis for estimating fat mass (FM), percent fat mass and fat-free mass (BioElectrical Impedance Analyzer System, RJL Systems, Detroit, MI). On the second day, a hyperinsulinemic-euglycemic clamp was performed in conjunction with muscle biopsies during fasting and at 30 min of insulin stimulation. Blinding was used whenever possible. This included blinding the investigator to the individual being studied with regard to group allocation and blinding the investigator who assessed and analyzed the data with regard to group allocation.

Laboratory analyses

Routine laboratory tests were analyzed at the Biomedical Laboratory of the German Diabetes Center Düsseldorf as described before (*88*). The fibrosis index (FIB-4), as an estimate of liver fibrosis, was calculated from routine laboratory parameters using the equation age × aspartate aminotransferase/platelet count × square root (alanine aminotransferase) (*89*).

Hyperinsulinemic-euglycemic clamp test

After an overnight fast, a hyperinsulinemic-euglycemic clamp with infusion of D-[6,6-$^2H_2$] glucose and total duration of 240 min was performed as described before to measure insulin sensitivity (*45*). Briefly, the examination was started at −120 min by a primed/continuous infusion of D-[6,6-$^2H_2$] glucose (0.04 mg kg^{-1} min^{-1}), at 0 min a bolus/continuous insulin infusion (40 mud/m^2 · body surface area/min; human regular insulin, Inhuman Rapid, Sanofi, Frankfurt, Germany) commenced and continued until 120 min. Blood glucose concentration was measured every 5 min using a glucometer (EKF Boise, Hamm, Germany) and maintained at fasting glucose levels by adapting the glucose infusion rate using 20% glucose (B. Braun AG, Melsungen, Germany) enriched with 2% D-[6,6-$^2H_2$]glucose. Insulin sensitivity (*M* value) was assessed from mean glucose infusion rates during the last 30 min of the clamp and glucose space correction was applied. All blood samples were collected at timed intervals.

Whole-body glucose disposal was calculated as disappearance rate Rd. during clamp steady-state from atom percent enrichments of ^{2}H in plasma glucose (*90*) using Steele's steady-state equations (*91*). During insulin-stimulated clamp conditions, hepatic insulin sensitivity was assessed from the suppression of EGP, calculated as 100 − (mean clamp steady state EGP *100)/(pre-basal EGP at 0 min), respectively (*92*).

Indirect calorimetry

During the last 30 min before and during the clamp steady state, indirect calorimetry was performed using a ventilated hood on a Vmax Encore 29n machine (SensorMedix; Cardinal Health Germany, Norderstedt, Germany) equipped with a variable mass flow, an infrared CO_2 sensor, and an electrochemical O_2 sensor (*93*), according to the recommended best practice guidelines (*94*, *95*). After a resting period of 10 min, a canopy was positioned over the participant's head and the measurement was started with an initial 10-min accommodation and equilibration period. The initial period was followed by a 20-min recording period, while the person remained under strict resting conditions. Data readout (i.e., VCO_2 and VO_2) was set at the highest available frequency (three readouts/min), and subsequent calibration with normalization was performed as described (*93*). Metabolic flexibility and substrate utilization then were calculated according to Peronnet *et al.* (*96*). Validated formulas (*93*) were used to calculate glucose oxidation (GOX) and lipid oxidation (LOX), while NOXGD was assessed from the difference between Rd. and GOX.

MRS and MRI

All MRS and magnetic resonance imaging (MRI) measurements were performed on a 3-T whole-body MR scanner (Achieva X-series, Philips Healthcare, Best, The Netherlands). Clinical T2-weighted turbo spin-echo images were obtained in the transverse plane of the left leg for localization and repositioning of the voxels used for IMCT quantifications. ^{1}H-MRS was performed for measuring IMCT content using point-resolved spectroscopy sequence (repetition time/echo time = 2000/29 ms) in a volume of interest of 15 mm 12 mm15 mm within the m. vastus lateralis muscle. IMCT content was calculated from the peak area of IMCT-CH_2- (methylene) at 1.3 parts per million with respect to the water peak area and was corrected for T1 and T2 relaxation effects as suggested previously (*97*). Quantification was performed when the spectra yielded a clearly visible spectral separation of IMCT methylene signals following consensus recommendation (*97*).

Skeletal muscle biopsy

Muscle biopsies at the mid-thigh level of the m. vastus lateralis were taken in the overnight fasted state and 30 min into the clamp test under insulin stimulated conditions in line with previous studies of our group (*18*). Under local anesthesia, a modified Bergström needle with suction was used to retrieve around 500 mg of muscle tissue (*78*). The biopsy site was treated with wound closure strips, a plaster, and bandage. Muscle samples were immediately blotted free of extramyocellular tissue or blood, weighted, frozen in liquid nitrogen, and stored at −80°C for further analysis (mitochondrial content and bioactive lipids in the overnight fasted state, Western blotting both in the overnight fasted state and under insulin-stimulated conditions). A part of the sample taken in the overnight fasted state was either embedded for TEM histochemical analysis or used fresh for mitochondrial respiration measurements.

Transmission electron microscopy

Skeletal muscle tissue from m. vastus lateralis was fixed for 2 hours at room temperature (RT) by immersion in 2.5% glutaraldehyde in 0.19 M sodium cacodylate buffer at pH 7.4, postfixed in 1% reduced osmium tetroxide in aqua bidest for 60 min, and subsequently stained with 2% uranyl acetate in maleate buffer (pH 4.7). The specimens were dehydrated in graded ethanol and embedded in epoxy resin (*98*). Ultrathin sections were picked up onto formvarcarbon-coated grids, stained with lead citrate, and viewed and recorded by a

transmission electron microscope (TEM 910; Zeiss Elektronenmikroskopie, Oberkochen, Germany). Morphometric evaluation of mitochondrial volume density and lipid droplet volume density were performed via ImageJ [National Institutes of Health (NIH), Bethesda, MD, USA] using the point-counting method as previously described by Weibel (*99*).

Histochemical analysis

For immunofluorescence analysis of fiber types of the m. vastus lateralis, 7-μm-thick cryosections were cut and mounted on glass slides as described (*100*). The sections were air-dried for 15 min at RT and fixed thereafter with 3.7% formaldehyde in phosphate-buffered saline (PBS) for 30 min at 4°C. The sections were permeabilized with 0.25% Triton X-100 in PBS for 30 min at RT and incubated for 60 min at RT with antibodies against myosin heavy chain 1 (A4.840; Dev. Hybr. Bank, Iowa, USA) and laminin (L9393; Sigma-Aldrich, Zwijndrecht, The Netherlands). Subsequently, the sections were incubated for 90 min with the appropriate secondary antibodies conjugated with Alexa Fluor 555 and Alexa Fluor 350 (D3922; Thermo Fisher Scientific, Landsmeer, The Netherlands) at RT. Last, the sections were mounted with Mowiol and analyzed with a Nikon E800 fluorescence microscope (Nikon, Amsterdam, The Netherlands), coupled to a Nikon DS-Fi1c color CCD camera. All sections were individually assessed using ImageJ (NIH, Bethesda, MD, USA) (*101*) to distinguish muscle fiber types. Positive staining for major histocompatibility complex 1 identified type I muscle fibers, while unstained fibers were counted as type II fibers.

Mitochondrial function and content

Mitochondrial respiration was assessed by high-resolution respirometry using the Oxygraph 2 k (O2k, Oroboros instruments, Innsbruck, Austria) in permeabilized muscle fibers as described earlier after applying a sequential substrate-uncoupler-inhibitor protocol (*31*). In brief, skeletal muscle biopsy samples were permeabilized chemically with saponin for 30 min and transferred to the O2k chambers in duplicate. Defined respiratory states were obtained after applying malate (2 mM) and octanoylcarnitine (0.2 mM) to induce LEAK respiration followed by adenosine diphosphate (ADP, 2.5 mM) to support β-oxidation–linked respiration. This was followed by titrating glutamate (10 mM), succinate (10 mM), and ADP (5 mM) to obtain OXPHOS capacity and subsequent titration of oligomycin (2.5 μM) and stepwise (0.025 μM steps) titration of carbonyl cyanide-*p*-trifluoromethoxyphenylhydrazone to reach maximal respiratory capacity. The RCR was calculated as the ratio of mitochondrial respiration supporting adenosine triphosphate synthesis to that necessary to compensate for proton leak (*32*). The LCR as an indicator of mitochondrial proton leakage and coupling control was calculated using leak respiration divided by maximal respiratory capacity (*33*). CSA was assessed spectrophotometrically from a separate piece of muscle using a commercial kit (Citrate Synthase Assay Kit; Sigma-Aldrich, St. Louis, MO) and used as a marker for mitochondrial content. For analysis of mtDNA, DNA was extracted from muscle tissue using DNeasy Blood & Tissue kit (Qiagen, Düsseldorf, DE) following the manufacturer's instructions. Briefly, 15 mg of muscle tissue was lysed using ATL plus buffer and proteinase K at 56°C for 2 hours. Later, DNA was purified using DNeasy mini spin column and dissolved in 40 μl AE buffer. Last, DNA concentration and purity was determined by nanoplate reader (Tecan, Männedorf, CH) and diluted to 5 ng/μl using polymerase chain reaction (PCR)–grade H_2O. Mitochondrial DNA copy number was quantified with StepOne Plus PCR system (Applied Biosystems, Foster City, USA) using primers for nuclear gene lipoprotein lipase (LPL) (forward primer: CGAGTCGTCTTTCTCCTGATGAT reverse primer: TTCTGGATTCCAATGCTTCGA) and mitochondrial gene NADH dehydrogenase subunit 1 (ND1) (forward primers: CCCTAAAACCCGCCACATCT reverse primers: GAGCGATGGTGAGAGCTAAGGT). DNA copy number for each gene was determined by comparing log-linear standard curves created using plasmid for LPL and ND1 (OriGene, Maryland, USA). Mitochondrial DNA copy number was expressed as the logarithm of mitochondrial to nuclear DNA ratio as previously described (*102*). A melting curve was created to ensure primer specificity. Each sample was measured in duplicate. Inter-run calibrator was used to account for between-run differences.

Five-compartment ultracentrifugation fractionation and DAG stereoisomer separation and quantitation

Tissue was homogenized and fractionated into five compartments as described earlier (*38*). As reported previously (*103*), subcellular fraction purity of vastus lateralis muscle samples was evaluated by immunoblotting for the following marker proteins (fig. S3): Na-K adenosine triphosphatase (ATPase) (sarcolemma) antibody, Abcam, #ab7671; citrate synthase (mitochondria) antibody, Santa Cruz Biotechnology, #sc-390693; calnexin (endoplasmic reticulum) antibody, Abcam, #ab22595; perilipin (lipid droplet) antibody, Cell Signaling Technology, #9349; and glyceraldehyde-3-phosphate dehydrogenase (GAPDH) (cytosol) antibody, Cell Signaling Technology, #5174. Chiral analysis of DAG were performed by LC-MS/MS using electrospray ionization on an AB Sciex Qtrap 6500 interfaced to Shimadzu UFLC with 2 LC-20 AD pumps (and degassers), SIL-20 AC xR autosampler. Chromatographic separation was performed using Luna 5u Silica (100 A, 250 mm by 2.0 mm) and LUX 5u Cellulose-1 (250 mm by 4.6 mm) columns connected in series with an isocratic solvent of hexane:isoproponal (300:7) with a flow rate of 0.6 ml/min. Triacylglycerols (TAG) elute between ~4 and 8 min, and DAG elute between ~11 and 17 min. For DAG with the same fatty acid composition, the order of elution was 1,3-DAG - > 2,3-DAG - > 1,2-DAG. For any specific stereoisomer (i.e., 1,2-DAG, 2,3-DAG, or 1,3-DAG) the order of elution generally increases with the degree of unsaturation. For example, C18:1 C18:1 - > C18:1 C18:2 - > C18:2 C18:2. Standards were used to establish retention times, matrix effects, and response relative to the internal standard (C17, C17-DAG). However, the position of the fatty acids on the DAG have not been established. For example, for the 1,2-DAG assigned as C18:0 C16:0, C16:0 could be on either the 1 or the 2 positions. In the process of optimization, it was found that the use of cartridges (e.g., DiOH) or silica thin-layer chromatography plates to preseparate the DAG from TAG results leads to intramolecular transesterification (e.g., the preseparation of a 1,2-DAG, will produce a mixture of 1,2-, 2,3-, and 1,3-DAG). Thus, no additional separation steps following centrifugation to obtain cellular fraction were done b LC-MS/MS analysis.

Western blotting

Expression levels of proteins of interest were assessed by Western blot (*104*). Proteins were extracted from approximately 30 mg of frozen skeletal muscle and homogenized in 300 μl of lysis buffer (25 mM tris-HCl, 1 mM EDTA, 150 mM NaCl, and 0.20% NP-40) with protease (cOmplete Tablets, EASYpack, Roche Diagnostics) and phosphatase (PhosSTOP, EASYpack, Roche Diagnostics) inhibitors for extraction of total soluble proteins. The samples were shaken three times for 1 min at 20 Hz in a Tissue Lyzer and centrifuged (13,000 rpm for 15 min at 4°C) to pellet insolubilized material.

GLUT4 protein content was assessed from lysate, and as a marker of activation, PKCθ and PKCε activities were assessed from the ratios of the respective protein contents in membrane and cytosol fractions upon differential centrifugation. The tissue was homogenized in 300 μl of lysis buffer with protease and phosphatase inhibitors. The homogenate was centrifuged (100,000*g* for 1 hour at 4°C), and the supernatant containing the cytosolic fraction was transferred to a fresh tube and frozen at −80°C, while the pellet was dissolved in 110 μl of buffer B (250 mM tris-HCL, 1 mM EDTA, 0.25 mM EGTA, and 2% Triton X-100) using a homogenizer. A second centrifugation step (100,000*g* for 1 hour at 4°C) was performed, and the supernatant (membrane fraction) was collected and stored at −80°C as well.

The concentration of the extracted proteins was determined in the supernatant using the bicinchoninic acid assay kit. Aliquots of 30 μg of total proteins, as well as cytosolic and membrane fractions, were diluted four times with the loading buffer [0.35 M tris-HCl (pH 6.8), 10% SDS, 30% glycerol, 0.6 M dithiothreitol, and 0.175 mM bromophenol blue) and then loaded onto an SDS-PAGE (4 to 20% Mini-PROTEAN TGX Precast Protein Gels, Bio-Rad, CA, USA). Following electrophoresis, a semidry blotting to a polyvinylidene difluoride membrane was performed at 8 mA/cm^2 for 30 min. After blocking the membranes for 2 hour at RT using the blocking solution [5% milk in tris-buffered saline–Tween (TBS-T)], the membranes were incubated with the primary antibodies diluted 1:1000 in 5% milk or bovine serum albumin in TBS-T according to the manufacturer, in combination with the respective horseradish peroxidase (HRP)–conjugated secondary anti-rabbit antibody, diluted 1:2500, or anti-mouse diluted 1:1000. The membranes were finally coated with Immobilon Western Chemiluminescent HRP Substrate (Millipore), and the proteins were detected using a Bio-Rad ChemiDocTM MP Imaging System in combination with the software ImageLab 6.0.1 (Bio-Rad 199 Laboratories) for densitometric analysis. For analysis and comparison of the protein expression on different gels, an inter-run calibrator was loaded as reference sample on each gel to correct for run-to-run variation (*105*). Primary antibodies were purchased from Cell Signaling Technology: Akt (9272); phospho-Ser^{473}-Akt (9271); HKI (2024); HK II (2106); NF-κB (8242); phospho–NF-κB (3033); GAPDH (2118) as housekeeping protein for the soluble and cytosolic fractions. PKCθ (610090) and PKCε (610086) were obtained from BD Biosciences, Calpain 1 (VMA00353) and Calpain 2 (VMA00164) from Bio-Rad, and Na^+,K^+-ATPase (Ab76020), used as loading control for the membrane fraction, from Abcam. Data are expressed in arbitrary units and normalized to housekeeping protein.

Statistics

Data are presented as means ± SEM or median (25th, 75th percentiles) in case of skewed distributed variables, as appropriate and as percentages (%). Group differences were analyzed by two-way analysis of variance (ANOVA), and the Tukey-Kramer method was used to adjust *P* values for multiple comparisons or pairwise comparisons of three groups. Pearson's linear regression analysis was performed to identify correlations between variables. Differences were considered significant at $P < 0.05$, and a two-sided approach was used. Results from DAG and CER molecular species were adjusted for age and sex, which have been shown to affect lipid species (*106*). Subgroup and sex-specific analyses were performed in an identical manner as indicated above. To determine whether DAG or ceramide species, localization and insulin sensitivity are associated with physical fitness within a subgroup, VO_2max was set as the dependent variable. Missing values were not imputed for any analyses, and data were computed according to available case analysis. Sex was based on self-reporting, and both male and female individuals were included into this study, but this study was not designed and powered to assess sex-specific differences.

Sample size and power calculation

The number of cases for the main study was calculated using a power analysis (G*Power version 3.1.9.2) assuming the following parameters: mean IMCT levels in ATHLs, 9000 arbitrary units (AU) (SD, 3000 AU); untrained, insulin-sensitive control participants, 6000 A.U. (SD, 1000 A.U.); effect size, 1.2; $Z\alpha = 1.96$ (95%, two-sided); and $Z\beta = 0.84$ (80%, one-sided) according to the tolerable limits for type 1 and type 2 errors of the respective main target parameter to define the groups (IMCT) based on previous studies (*21*). The power analysis resulted in a sample size of at least 12 individuals per group for a two-sided test. IMCTs are a distinctive parameter for differentiating the groups. With a drop-out rate of about 10% and the assumption that the investigation of more heterogeneous groups in the reference study would result in a higher spread of the measured values, a number of 15 participants per group and subproject was set.

Supplementary Materials

This PDF file includes:

Figs. S1 to S8

Tables S1 and S2

REFERENCES AND NOTES

1. M. Krssak, K. Falk Petersen, A. Dresner, L. DiPietro, S. M. Vogel, D. L. Rothman, M. Roden, G. I. Shulman, Intramyocellular lipid concentrations are correlated with insulin sensitivity in humans: A 1H NMR spectroscopy study. *Diabetologia* **42**, 113–116 (1999).
2. K. Levin, H. Daa Schroeder, F. P. Alford, H. Beck-Nielsen, Morphometric documentation of abnormal intramyocellular fat storage and reduced glycogen in obese patients with type II diabetes. *Diabetologia* **44**, 824–833 (2001).
3. G. Perseghin, G. Lattuada, F. De Cobelli, F. Ragogna, G. Ntali, A. Esposito, E. Belloni, T. Canu, I. Terruzzi, P. Scifo, A. Del Maschio, L. Luzi, Habitual physical activity is associated with intrahepatic fat content in humans. *Diabetes Care* **30**, 683–688 (2007).
4. J. J. Dube, F. Amati, M. Stefanovic-Racic, F. G. Toledo, S. E. Sauers, B. H. Goodpaster, Exercise-induced alterations in intramyocellular lipids and insulin resistance: The athlete's paradox revisited. *Am. J. Physiol. Endocrinol. Metab.* **294**, E882–E888 (2008).
5. B. H. Goodpaster, J. He, S. Watkins, D. E. Kelley, Skeletal muscle lipid content and insulin resistance: Evidence for a paradox in endurance-trained athletes. *J. Clin. Endocrinol. Metab.* **86**, 5755–5761 (2001).
6. L. J. van Loon, B. H. Goodpaster, Increased intramuscular lipid storage in the insulin-resistant and endurance-trained state. *Pflugers Arch.* **451**, 606–616 (2006).
7. K. F. Petersen, S. Dufour, D. Befroy, R. Garcia, G. I. Shulman, Impaired mitochondrial activity in the insulin-resistant offspring of patients with type 2 diabetes. *N. Engl. J. Med.* **350**, 664–671 (2004).
8. K. F. Petersen, D. Befroy, S. Dufour, J. Dziura, C. Ariyan, D. L. Rothman, L. DiPietro, G. W. Cline, G. I. Shulman, Mitochondrial dysfunction in the elderly: Possible role in insulin resistance. *Science* **3**, 1140–1142 (2003).
9. D. E. Befroy, K. F. Petersen, S. Dufour, G. F. Mason, R. A. de Graaf, D. L. Rothman, G. I. Shulman, Impaired mitochondrial substrate oxidation in muscle of insulin-resistant offspring of type 2 diabetic patients. *Diabetes* **56**, 1376–1381 (2007).
10. H. Y. Lee, C. S. Choi, A. L. Birkenfeld, T. C. Alves, F. R. Jornayvaz, M. J. Jurczak, D. Zhang, D. K. Woo, G. S. Shadel, W. Ladiges, P. S. Rabinovitch, J. H. Santos, K. F. Petersen, V. T. Samuel, G. I. Shulman, Targeted expression of catalase to mitochondria prevents age-associated reductions in mitochondrial function and insulin resistance. *Cell Metab.* **12**, 668–674 (2010).
11. C. R. Hancock, D. H. Han, M. Chen, S. Terada, T. Yasuda, D. C. Wright, J. O. Holloszy, High-fat diets cause insulin resistance despite an increase in muscle mitochondria. *Proc. Natl. Acad. Sci. U.S.A.* **105**, 7815–7820 (2008).
12. J. D. Song, T. C. Alves, D. E. Befroy, R. J. Perry, G. F. Mason, X. M. Zhang, A. Munk, Y. Zhang, D. Zhang, G. W. Cline, D. L. Rothman, K. F. Petersen, G. I. Shulman, Dissociation of muscle

insulin resistance from alterations in mitochondrial substrate preference. *Cell Metab.* **32**, 726–735.e5 (2020).
13. M. Apostolopoulou, L. Mastrototaro, S. Hartwig, D. Pesta, K. Straßburger, E. de Filippo, T. Jelenik, Y. Karusheva, S. Gancheva, D. Markgraf, C. Herder, K. S. Nair, A. S. Reichert, S. Lehr, K. Müssig, H. Al-Hasani, J. Szendroedi, M. Roden, Metabolic responsiveness to training depends on insulin sensitivity and protein content of exosomes in insulin-resistant males. *Sci. Adv.* **7**, eabi9551 (2021).
14. S. Gancheva, T. Jelenik, E. Alvarez-Hernandez, M. Roden, Interorgan metabolic crosstalk in human insulin resistance. *Physiol. Rev.* **98**, 1371–1415 (2018).
15. M. C. Petersen, G. I. Shulman, Mechanisms of insulin action and insulin resistance. *Physiol. Rev.* **98**, 2133–2223 (2018).
16. B. C. Bergman, J. T. Brozinick, A. Strauss, S. Bacon, A. Kerege, H. H. Bui, P. Sanders, P. Siddall, T. Wei, M. K. Thomas, M. S. Kuo, L. Perreault, Muscle sphingolipids during rest and exercise: A C18:0 signature for insulin resistance in humans. *Diabetologia* **59**, 785–798 (2016).
17. Y. Li, T. J. Soos, X. Li, J. Wu, M. Degennaro, X. Sun, D. R. Littman, M. J. Birnbaum, R. D. Polakiewicz, Protein kinase C Theta inhibits insulin signaling by phosphorylating IRS1 at Ser(1101). *J. Biol. Chem.* **279**, 45304–45307 (2004).
18. J. Szendroedi, T. Yoshimura, E. Phielix, C. Koliaki, M. Marcucci, D. Zhang, T. Jelenik, J. Müller, C. Herder, P. Nowotny, G. I. Shulman, M. Roden, Role of diacylglycerol activation of PKCθ in lipid-induced muscle insulin resistance in humans. *Proc. Natl. Acad. Sci. U.S.A.* **111**, 9597–9602 (2014).
19. J. M. Adams II, T. Pratipanawatr, R. Berria, E. Wang, R. A. DeFronzo, M. C. Sullards, L. J. Mandarino, Ceramide content is increased in skeletal muscle from obese insulin-resistant humans. *Diabetes* **53**, 25–31 (2004).
20. S. Stratford, D. B. DeWald, S. A. Summers, Ceramide dissociates 3′-phosphoinositide production from pleckstrin homology domain translocation. *Biochem. J.* **354**, 359–368 (2001).
21. F. Amati, J. J. Dubé, E. Alvarez-Carnero, M. M. Edreira, P. Chomentowski, P. M. Coen, G. E. Switzer, P. E. Bickel, M. Stefanovic-Racic, F. G. Toledo, B. H. Goodpaster, Skeletal muscle triglycerides, diacylglycerols, and ceramides in insulin resistance: Another paradox in endurance-trained athletes? *Diabetes* **60**, 2588–2597 (2011).
22. S. U. Jayasinghe, A. T. Tankeu, F. Amati, Reassessing the role of diacylglycerols in insulin resistance. *Trends Endocrinol. Metab.* **30**, 618–635 (2019).
23. J. L. Cantley, T. Yoshimura, J. P. G. Camporez, D. Zhang, F. R. Jornayvaz, N. Kumashiro, F. Guebre-Egziabher, M. J. Jurczak, M. Kahn, B. A. Guigni, J. Serr, J. Hankin, R. C. Murphy, G. W. Cline, S. Bhanot, V. P. Manchem, J. M. Brown, V. T. Samuel, G. I. Shulman, CGI-58 knockdown sequesters diacylglycerols in lipid droplets/ER-preventing diacylglycerol-mediated hepatic insulin resistance. *Proc. Natl. Acad. Sci. U.S.A.* **110**, 1869–1874 (2013).
24. L. Perreault, S. A. Newsom, A. Strauss, A. Kerege, D. E. Kahn, K. A. Harrison, J. K. Snell-Bergeon, T. Nemkov, A. D'Alessandro, M. R. Jackman, P. S. MacLean, B. C. Bergman, Intracellular localization of diacylglycerols and sphingolipids influences insulin sensitivity and mitochondrial function in human skeletal muscle. *JCI Insight* **3**, e96805 (2018).
25. K. Lyu, Y. Zhang, D. Zhang, M. Kahn, K. W. Ter Horst, M. R. S. Rodrigues, R. C. Gaspar, S. M. Hirabara, P. K. Luukkonen, S. Lee, S. Bhanot, J. Rinehart, N. Blume, M. G. Rasch, M. J. Serlie, J. S. Bogan, G. W. Cline, V. T. Samuel, G. I. Shulman, A membrane-bound diacylglycerol species induces PKCε-mediated hepatic insulin resistance. *Cell Metab.* **32**, 654–664.e5 (2020).
26. M. Skovbro, M. Baranowski, C. Skov-Jensen, A. Flint, F. Dela, J. Gorski, J. W. Helge, Human skeletal muscle ceramide content is not a major factor in muscle insulin sensitivity. *Diabetologia* **51**, 1253–1260 (2008).
27. C. L. Kien, J. Y. Bunn, M. E. Poynter, R. Stevens, J. Bain, O. Ikayeva, N. K. Fukagawa, C. M. Champagne, K. I. Crain, T. R. Koves, D. M. Muoio, A lipidomics analysis of the relationship between dietary fatty acid composition and insulin sensitivity in young adults. *Diabetes* **62**, 1054–1063 (2013).
28. R. A. DeFronzo, J. D. Tobin, R. Andres, Glucose clamp technique: A method for quantifying insulin secretion and resistance. *Am. J. Physiol.* **237**, E214–E223 (1979).
29. J. E. Galgani, C. Moro, E. Ravussin, Metabolic flexibility and insulin resistance. *Am. J. Physiol. Endocrinol. Metab.* **295**, E1009–E1017 (2008).
30. A. D. Association, 2. Classification and diagnosis of diabetes: Standards of medical care in diabetes-2020. *Diabetes Care* **43**, S14–S31 (2020).
31. D. Pesta, E. Gnaiger, High-resolution respirometry: OXPHOS protocols for human cells and permeabilized fibers from small biopsies of human muscle. *Methods Mol. Biol.* **810**, 25–58 (2012).
32. M. D. Brand, D. G. Nicholls, Assessing mitochondrial dysfunction in cells. *Biochem. J.* **435**, 297–312 (2011).
33. E. Gnaiger, Capacity of oxidative phosphorylation in human skeletal muscle: New perspectives of mitochondrial physiology. *Int. J. Biochem. Cell Biol.* **41**, 1837–1845 (2009).
34. S. Larsen, J. Nielsen, C. N. Hansen, L. B. Nielsen, F. Wibrand, N. Stride, H. D. Schroder, R. Boushel, J. W. Helge, F. Dela, M. Hey-Mogensen, Biomarkers of mitochondrial content in skeletal muscle of healthy young human subjects. *J. Physiol.* **590**, 3349–3360 (2012).
35. A. N. Malik, A. Czajka, Is mitochondrial DNA content a potential biomarker of mitochondrial dysfunction? *Mitochondrion* **13**, 481–492 (2013).
36. P. Puigserver, B. M. Spiegelman, Peroxisome proliferator-activated receptor-gamma coactivator 1α (PGC-1α): Transcriptional coactivator and metabolic regulator. *Endocr. Rev.* **24**, 78–90 (2003).
37. B. Nowotny, L. Zahiragic, A. Bierwagen, S. Kabisch, J. B. Groener, P. J. Nowotny, A. K. Fleitmann, C. Herder, G. Pacini, I. Erlund, R. Landberg, H.-U. Haering, A. F. H. Pfeiffer, P. P. Nawroth, M. Roden, Low-energy diets differing in fibre, red meat and coffee intake equally improve insulin sensitivity in type 2 diabetes: A randomised feasibility trial. *Diabetologia* **58**, 255–264 (2015).
38. K. Lyu, Y. Zhang, D. Zhang, M. Kahn, K. W. Ter Horst, M. R. S. Rodrigues, R. C. Gaspar, S. M. Hirabara, P. K. Luukkonen, S. Lee, S. Bhanot, J. Rinehart, N. Blume, M. G. Rasch, M. J. Serlie, J. S. Bogan, G. W. Cline, V. T. Samuel, G. I. Shulman, A membrane-bound diacylglycerol species induces PKCe-mediated hepatic insulin resistance. *Cell Metab.* **32**, 654–664.e5 (2020).
39. J. A. Chavez, S. A. Summers, A ceramide-centric view of insulin resistance. *Cell Metab.* **15**, 585–594 (2012).
40. C. Schmitz-Peiffer, C. L. Browne, N. D. Oakes, A. Watkinson, D. J. Chisholm, E. W. Kraegen, T. J. Biden, Alterations in the expression and cellular localization of protein kinase C isozymes epsilon and theta are associated with insulin resistance in skeletal muscle of the high-fat-fed rat. *Diabetes* **46**, 169–178 (1997).
41. S. E. Shoelson, J. Lee, M. Yuan, Inflammation and the IKKβ/IκB/NF-κB axis in obesity- and diet-induced insulin resistance. *Int. J. Obes. Relat. Metab. Disord.* **27**, S49–S52 (2003).
42. D. E. Befroy, K. F. Petersen, S. Dufour, G. F. Mason, D. L. Rothman, G. I. Shulman, Increased substrate oxidation and mitochondrial uncoupling in skeletal muscle of endurance-trained individuals. *Proc. Natl. Acad. Sci. U.S.A.* **105**, 16701–16706 (2008).
43. A. I. Schmid, J. Szendroedi, M. Chmelik, M. Krssák, E. Moser, M. Roden, Liver ATP synthesis is lower and relates to insulin sensitivity in patients with type 2 diabetes. *Diabetes Care* **34**, 448–453 (2011).
44. B. B. Kahn, J. S. Flier, Obesity and insulin resistance. *J. Clin. Invest.* **106**, 473–481 (2000).
45. E. Phielix, P. Begovatz, S. Gancheva, A. Bierwagen, E. Kornips, G. Schaart, M. K. C. Hesselink, P. Schrauwen, M. Roden, Athletes feature greater rates of muscle glucose transport and glycogen synthesis during lipid infusion. *JCI insight* **4**, e127928 (2019).
46. G. D. Wadley, N. Konstantopoulos, L. Macaulay, K. F. Howlett, A. Garnham, M. Hargreaves, D. Cameron-Smith, Increased insulin-stimulated Akt pSer473 and cytosolic SHP2 protein abundance in human skeletal muscle following acute exercise and short-term training. *J. Appl. Physiol.* **102**, 1624–1631 (2007).
47. A. Deshmukh, V. G. Coffey, Z. Zhong, A. V. Chibalin, J. A. Hawley, J. R. Zierath, Exercise-induced phosphorylation of the novel Akt substrates AS160 and filamin A in human skeletal muscle. *Diabetes* **55**, 1776–1782 (2006).
48. K. Højlund, J. B. Birk, D. K. Klein, K. Levin, A. J. Rose, B. F. Hansen, J. N. Nielsen, H. Beck-Nielsen, J. F. Wojtaszewski, Dysregulation of glycogen synthase COOH- and NH2-terminal phosphorylation by insulin in obesity and type 2 diabetes mellitus. *J. Clin. Endocrinol. Metab.* **94**, 4547–4556 (2009).
49. D. Cozzone, S. Fröjdö, E. Disse, C. Debard, M. Laville, L. Pirola, H. Vidal, Isoform-specific defects of insulin stimulation of Akt/protein kinase B (PKB) in skeletal muscle cells from type 2 diabetic patients. *Diabetologia* **51**, 512–521 (2008).
50. E. Carvalho, B. Eliasson, C. Wesslau, U. Smith, Impaired phosphorylation and insulin-stimulated translocation to the plasma membrane of protein kinase B/Akt in adipocytes from type II diabetic subjects. *Diabetologia* **43**, 1107–1115 (2000).
51. J. Décombaz, B. Schmitt, M. Ith, B. Decarli, P. Diem, R. Kreis, H. Hoppeler, C. Boesch, Postexercise fat intake repletes intramyocellular lipids but no faster in trained than in sedentary subjects. *Am. J. Physiol. Regul. Integr. Comp. Physiol.* **281**, R760–R769 (2001).
52. L. J. van Loon, R. Koopman, R. Manders, W. van der Weegen, G. P. van Kranenburg, H. A. Keizer, Intramyocellular lipid content in type 2 diabetes patients compared with overweight sedentary men and highly trained endurance athletes. *Am. J. Physiol. Endocrinol. Metab.* **287**, E558–E565 (2004).
53. M. Roden, G. I. Shulman, The integrative biology of type 2 diabetes. *Nature* **576**, 51–60 (2019).
54. D. Pesta, F. Hoppel, C. Macek, H. Messner, M. Faulhaber, C. Kobel, W. Parson, M. Burtscher, M. Schocke, E. Gnaiger, Similar qualitative and quantitative changes of mitochondrial respiration following strength and endurance training in normoxia and hypoxia in sedentary humans. *Am. J. Physiol. Regul. Integr. Comp. Physiol.* **301**, R1078–R1087 (2011).
55. M. A. Tarnopolsky, C. D. Rennie, H. A. Robertshaw, S. N. Fedak-Tarnopolsky, M. C. Devries, M. J. Hamadeh, Influence of endurance exercise training and sex on intramyocellular lipid and mitochondrial ultrastructure, substrate use, and mitochondrial enzyme activity. *Am. J. Physiol. Regul. Integr. Comp. Physiol.* **292**, R1271–R1278 (2007).
56. G. Perseghin, P. Scifo, M. Danna, A. Battezzati, S. Benedini, E. Meneghini, A. Del Maschio, L. Luzi, Normal insulin sensitivity and IMCL content in overweight humans are associated with higher fasting lipid oxidation. *Am. J. Physiol. Endocrinol. Metab.* **283**, E556–E564 (2002).

57. H. E. Koh, J. Nielsen, B. Saltin, H. C. Holmberg, N. Ørtenblad, Pronounced limb and fibre type differences in subcellular lipid droplet content and distribution in elite skiers before and after exhaustive exercise. *J. Physiol.* **595**, 5781–5795 (2017).
58. N. Luden, E. Hayes, K. Minchev, E. Louis, U. Raue, T. Conley, S. Trappe, Skeletal muscle plasticity with marathon training in novice runners. *Scand. J. Med. Sci. Sports* **22**, 662–670 (2012).
59. E. F. Coyle, M. E. Feltner, S. A. Kautz, M. T. Hamilton, S. J. Montain, A. M. Baylor, L. D. Abraham, G. W. Petrek, Physiological and biomechanical factors associated with elite endurance cycling performance. *Med. Sci. Sports Exerc.* **23**, 93–107 (1991).
60. J. He, S. Watkins, D. E. Kelley, Skeletal muscle lipid content and oxidative enzyme activity in relation to muscle fiber type in type 2 diabetes and obesity. *Diabetes* **50**, 817–823 (2001).
61. S. R. Costford, S. Bajpeyi, M. Pasarica, D. C. Albarado, S. C. Thomas, H. Xie, T. S. Church, S. A. Jubrias, K. E. Conley, S. R. Smith, Skeletal muscle NAMPT is induced by exercise in humans. *Am. J. Physiol. Endocrinol. Metab.* **298**, E117–E126 (2010).
62. R. A. Jacobs, C. Lundby, Mitochondria express enhanced quality as well as quantity in association with aerobic fitness across recreationally active individuals up to elite athletes. *J. Appl. Physiol.* **114**, 344–350 (2013).
63. A. Puntschart, H. Claassen, K. Jostarndt, H. Hoppeler, R. Billeter, mRNAs of enzymes involved in energy metabolism and mtDNA are increased in endurance-trained athletes. *Am. J. Physiol.* **269**, C619–C625 (1995).
64. G. Layec, A. Bringard, Y. Le Fur, J. P. Micallef, C. Vilmen, S. Perrey, P. J. Cozzone, D. Bendahan, Mitochondrial coupling and contractile efficiency in humans with high and low V˙O2peaks. *Med. Sci. Sports Exerc.* **48**, 811–821 (2016).
65. A. S. Mathai, A. Bonen, C. R. Benton, D. L. Robinson, T. E. Graham, Rapid exercise-induced changes in PGC-1alpha mRNA and protein in human skeletal muscle. *J. Appl. Physiol.* **105**, 1098–1105 (2008).
66. J. Kuang, C. McGinley, M. J. Lee, N. J. Saner, A. Garnham, D. J. Bishop, Interpretation of exercise-induced changes in human skeletal muscle mRNA expression depends on the timing of the post-exercise biopsies. *PeerJ* **10**, e12856 (2022).
67. B. C. Bergman, D. M. Hunerdosse, A. Kerege, M. C. Playdon, L. Perreault, Localisation and composition of skeletal muscle diacylglycerol predicts insulin resistance in humans. *Diabetologia* **55**, 1140–1150 (2012).
68. J. W. Jocken, G. H. Goossens, H. Boon, R. R. Mason, Y. Essers, B. Havekes, M. J. Watt, L. J. van Loon, E. E. Blaak, Insulin-mediated suppression of lipolysis in adipose tissue and skeletal muscle of obese type 2 diabetic men and men with normal glucose tolerance. *Diabetologia* **56**, 2255–2265 (2013).
69. R. C. Gaspar, K. Lyu, B. T. Hubbard, B. P. Leitner, P. K. Luukkonen, S. M. Hirabara, I. Sakuma, A. Nasiri, D. Zhang, M. Kahn, G. W. Cline, J. R. Pauli, R. J. Perry, K. F. Petersen, G. I. Shulman, Distinct subcellular localisation of intramyocellular lipids and reduced PKCε/PKCθ activity preserve muscle insulin sensitivity in exercise-trained mice. *Diabetologia* **66**, 567–578 (2023).
70. R. Wagner, M. Heni, A. G. Tabák, J. Machann, F. Schick, E. Randrianarisoa, M. Hrabě de Angelis, A. L. Birkenfeld, N. Stefan, A. Peter, H. U. Häring, A. Fritsche, Pathophysiology-based subphenotyping of individuals at elevated risk for type 2 diabetes. *Nat. Med.* **27**, 49–57 (2021).
71. O. P. Zaharia, K. Strassburger, A. Strom, G. J. Bönhof, Y. Karusheva, S. Antoniou, K. Bódis, D. F. Markgraf, V. Burkart, K. Müssig, J. H. Hwang, O. Asplund, L. Groop, E. Ahlqvist, J. Seissler, P. Nawroth, S. Kopf, S. M. Schmid, M. Stumvoll, A. F. H. Pfeiffer, S. Kabisch, S. Tselmin, H. U. Häring, D. Ziegler, O. Kuss, J. Szendroedi, M. Roden, Risk of diabetes-associated diseases in subgroups of patients with recent-onset diabetes: A 5-year follow-up study. *Lancet Diabetes Endocrinol.* **7**, 684–694 (2019).
72. D. E. Goll, V. F. Thompson, H. Li, W. Wei, J. Cong, The calpain system. *Physiol. Rev.* **83**, 731–801 (2003).
73. C. M. Cressman, P. S. Mohan, R. A. Nixon, T. B. Shea, Proteolysis of protein kinase C: mM and microM calcium-requiring calpains have different abilities to generate, and degrade the free catalytic subunit, protein kinase M. *FEBS Lett.* **367**, 223–227 (1995).
74. M. Savart, C. Verret, D. Dutaud, K. Touyarot, N. Elamrani, A. Ducastaing, Isolation and identification of a mu-calpain-protein kinase C alpha complex in skeletal muscle. *FEBS Lett.* **359**, 60–64 (1995).
75. Y. C. Liang, J. Y. Yeh, N. E. Forsberg, B. R. Ou, Involvement of mu- and m-calpains and protein kinase C isoforms in L8 myoblast differentiation. *Int. J. Biochem. Cell Biol.* **38**, 662–670 (2006).
76. A. Kishimoto, K. Mikawa, K. Hashimoto, I. Yasuda, S. Tanaka, M. Tominaga, T. Kuroda, Y. Nishizuka, Limited proteolysis of protein kinase C subspecies by calcium-dependent neutral protease (calpain). *J. Biol. Chem.* **264**, 4088–4092 (1989).
77. K. D. Gejl, E. P. Andersson, J. Nielsen, H. C. Holmberg, N. Ørtenblad, Effects of acute exercise and training on the sarcoplasmic reticulum Ca(2+) release and uptake rates in highly trained endurance athletes. *Front. Physiol.* **11**, 810 (2020).
78. J. Szendroedi, T. Yoshimura, E. Phielix, C. Koliaki, M. Marcucci, D. Zhang, T. Jelenik, J. Muller, C. Herder, P. Nowotny, G. I. Shulman, M. Roden, Role of diacylglycerol activation of PKCtheta in lipid-induced muscle insulin resistance in humans. *Proc. Natl. Acad. Sci. U.S.A.* **111**, 9597–9602 (2014).
79. M. J. Watt, A. Hevener, G. I. Lancaster, M. A. Febbraio, Ciliary neurotrophic factor prevents acute lipid-induced insulin resistance by attenuating ceramide accumulation and phosphorylation of c-Jun N-terminal kinase in peripheral tissues. *Endocrinology* **147**, 2077–2085 (2006).
80. M. Röhl, M. Pasparakis, S. Baudler, J. Baumgartl, D. Gautam, M. Huth, R. De Lorenzi, W. Krone, K. Rajewsky, J. C. Brüning, Conditional disruption of IkappaB kinase 2 fails to prevent obesity-induced insulin resistance. *J. Clin. Invest.* **113**, 474–481 (2004).
81. R. G. Shulman, G. Bloch, D. L. Rothman, In vivo regulation of muscle glycogen synthase and the control of glycogen synthesis. *Proc. Natl. Acad. Sci. U.S.A.* **92**, 8535–8542 (1995).
82. P. H. Andersen, S. Lund, O. Schmitz, S. Junker, B. B. Kahn, O. Pedersen, Increased insulin-stimulated glucose uptake in athletes: The importance of GLUT4 mRNA, GLUT4 protein and fibre type composition of skeletal muscle. *Acta Physiol. Scand.* **149**, 393–404 (1993).
83. R. S. Biensø, S. Ringholm, K. Kiilerich, N. J. Aachmann-Andersen, R. Krogh-Madsen, B. Guerra, P. Plomgaard, G. van Hall, J. T. Treebak, B. Saltin, C. Lundby, J. A. Calbet, H. Pilegaard, J. F. Wojtaszewski, GLUT4 and glycogen synthase are key players in bed rest-induced insulin resistance. *Diabetes* **61**, 1090–1099 (2012).
84. P. T. Fueger, J. Shearer, T. M. Krueger, K. A. Posey, D. P. Bracy, S. Heikkinen, M. Laakso, J. N. Rottman, D. H. Wasserman, Hexokinase II protein content is a determinant of exercise endurance capacity in the mouse. *J. Physiol.* **566**, 533–541 (2005).
85. H. Shimokata, D. C. Muller, J. L. Fleg, J. Sorkin, A. W. Ziemba, R. Andres, Age as independent determinant of glucose tolerance. *Diabetes* **40**, 44–51 (1991).
86. C. Aguer, C. S. McCoin, T. A. Knotts, A. B. Thrush, K. Ono-Moore, R. McPherson, R. Dent, D. H. Hwang, S. H. Adams, M. E. Harper, Acylcarnitines: Potential implications for skeletal muscle insulin resistance. *FASEB J.* **29**, 336–345 (2015).
87. R. M. Ross, ATS/ACCP statement on cardiopulmonary exercise testing. *Am. J. Respir. Crit. Care Med.* **167**, 1451; author reply 1451 (2003).
88. J. Szendroedi, A. Saxena, K. S. Weber, K. Strassburger, C. Herder, V. Burkart, B. Nowotny, A. Icks, O. Kuss, D. Ziegler, H. Al-Hasani, K. Mussig, M. Roden, GDS Group, Cohort profile: The German Diabetes Study (GDS). *Cardiovasc. Diabetol.* **15**, 59 (2016).
89. G. Xiao, S. Zhu, X. Xiao, L. Yan, J. Yang, G. Wu, Comparison of laboratory tests, ultrasound, or magnetic resonance elastography to detect fibrosis in patients with nonalcoholic fatty liver disease: A meta-analysis. *Hepatology* **66**, 1486–1501 (2017).
90. M. T. Ackermans, A. M. Pereira Arias, P. H. Bisschop, E. Endert, H. P. Sauerwein, J. A. Romijn, The quantification of gluconeogenesis in healthy men by $^{2}H_2O$ and [2-^{13}C]glycerol yields different results: Rates of gluconeogenesis in healthy men measured with $^{2}H_2O$ are higher than those measured with [2-^{13}C]glycerol. *J. Clin. Endocrinol. Metab.* **86**, 2220–2226 (2001).
91. R. Steele, Influences of glucose loading and of injected insulin on hepatic glucose output. *Ann. N. Y. Acad. Sci.* **82**, 420–430 (1959).
92. E. A. Hernandez, S. Kahl, A. Seelig, P. Begovatz, M. Irmler, Y. Kupriyanova, B. Nowotny, P. Nowotny, C. Herder, C. Barosa, F. Carvalho, J. Rozman, S. Neschen, J. G. Jones, J. Beckers, M. H. de Angelis, M. Roden, Acute dietary fat intake initiates alterations in energy metabolism and insulin resistance. *J. Clin. Invest.* **127**, 695–708 (2017).
93. P. Schadewaldt, B. Nowotny, K. Strassburger, J. Kotzka, M. Roden, Indirect calorimetry in humans: A postcalorimetric evaluation procedure for correction of metabolic monitor variability. *Am. J. Clin. Nutr.* **97**, 763–773 (2013).
94. C. Compher, D. Frankenfield, N. Keim, L. Roth-Yousey, G., Evidence analysis working, Best practice methods to apply to measurement of resting metabolic rate in adults: A systematic review. *J. Am. Diet. Assoc.* **106**, 881–903 (2006).
95. H. A. Haugen, L.-N. Chan, F. Li, Indirect calorimetry: A practical guide for clinicians. *Nutr. Clin. Pract.* **22**, 377–388 (2007).
96. F. Peronnet, D. Massicotte, Table of nonprotein respiratory quotient: An update. *Can. J. Sport Sci.* **16**, 23–29 (1991).
97. M. Krššák, L. Lindeboom, V. Schrauwen-Hinderling, L. S. Szczepaniak, W. Derave, J. Lundbom, D. Befroy, F. Schick, J. Machann, R. Kreis, C. Boesch, Proton magnetic resonance spectroscopy in skeletal muscle: Experts' consensus recommendations. *NMR Biomed.* **34**, e4266 (2021).
98. A. R. Spurr, A low-viscosity epoxy resin embedding medium for electron microscopy. *J. Ultrastruct. Res.* **26**, 31–43 (1969).
99. E. R. Weibel, Measuring through the microscope: Development and evolution of stereological methods. *J. Microsc.* **155**, 393–403 (1989).
100. A. Gemmink, S. Daemen, B. Brouwers, P. R. Huntjens, G. Schaart, E. Moonen-Kornips, J. Jorgensen, J. Hoeks, P. Schrauwen, M. K. C. Hesselink, Dissociation of intramyocellular lipid storage and insulin resistance in trained athletes and type 2 diabetes patients; involvement of perilipin 5? *J. Physiol.* **596**, 857–868 (2018).
101. C. A. Schneider, W. S. Rasband, K. W. Eliceiri, NIH Image to ImageJ: 25 years of image analysis. *Nat. Methods* **9**, 671–675 (2012).
102. S. Gancheva, S. Kahl, D. Pesta, L. Mastrototaro, B. Dewidar, K. Strassburger, E. Sabah, I. Esposito, J. Weiß, T. Sarabhai, M. Wolkersdorfer, T. Fleming, P. Nawroth, M. Zimmermann, A. S. Reichert, M. Schlensak, M. Roden, Impaired hepatic mitochondrial capacity in nonalcoholic steatohepatitis associated with type 2 diabetes. *Diabetes Care* **45**, 928–937 (2022).

103. M. C. Petersen, M. Yoshino, G. I. Smith, R. C. Gaspar, M. Kahn, D. Samovski, G. I. Shulman, S. Klein, Effect of weight loss on skeletal muscle bioactive lipids in people with obesity and type 2 diabetes. *Diabetes* **3**, 2055–2064 (2024).
104. T. Mahmood, P. C. Yang, Western blot: Technique, theory, and trouble shooting. *N. Am. J. Med. Sci.* **4**, 429–434 (2012).
105. K. Pafili, S. Kahl, L. Mastrototaro, K. Strassburger, D. Pesta, C. Herder, J. Pützer, B. Dewidar, M. Hendlinger, C. Granata, N. Saatmann, A. Yavas, S. Gancheva, G. Heilmann, I. Esposito, M. Schlensak, M. Roden, Mitochondrial respiration is decreased in visceral but not subcutaneous adipose tissue in obese individuals with fatty liver disease. *J. Hepatol.* **77**, 1504–1514 (2022).
106. D. Søgaard, M. Baranowski, S. Larsen, M. Taulo Lund, C. Munk Scheuer, C. Vestergaard Abildskov, S. Greve Dideriksen, F. Dela, J. Wulff Helge, Muscle-saturated bioactive lipids are increased with aging and influenced by high-intensity interval training. *Int. J. Mol. Sci.* **20**, (2019).

Acknowledgments: We would like to thank F. Ziehve, M. R. Do Fundo, D. Höhn, D. F. Markgraf, J. Leonhard, M. Kahn, D. Zhang, J.-H. Hwang, and M. K. C. Hesselink for excellent support and critical discussion of data as well as all study participants for participating in this study. Preliminary findings of this study have been presented during the Late Breaking Poster Session at the annual meeting of the American Diabetes Association in 2018. **Funding:** The German Diabetes Center is funded by the German Federal Ministry of Health and the Ministry of Culture and Science of the state of Northrhine-Westphalia and the German Federal Ministry of Education and Research (to the German Center for Diabetes Research). The study was in part also supported by grants from the from the European Community (HORIZON-HLTH-2022-STAYHLTH-02-01: Panel A) to the INTERCEPT-T2D consortium, the German Research Foundation (DFG; RTG/GRK 2576), the Schmutzler Stiftung, and grants from the National Institutes of Health/NIDDK (P30 DK045735, R01 DK133143). The funding sources had no role in study design, data collection, data analysis, data interpretation, or writing of the report. **Author contributions:** D.P., G.I.S., and M.R. designed and conceived the study. D.P., E.A.-S., T.S., Y.O.d.K., S.G., N.T., O.-P.Z., L.M., K.L., I.H., Y.O.d.K.-B., B.D., J.W., V.S.-H., D.Z., R.G., K.S., Y.K., H.A.-H., J.S., P.S., and E.P. designed, performed, and contributed to experiments. D.P. and K.S. analyzed the data, and K.S. assisted with biostatistics and bioinformatics analysis. D.P. and M.R. wrote and edited the manuscript with assistance from the other authors. All authors reviewed and approved the final version of the manuscript. **Competing interests:** M.R. received personal fees for lectures or advisory boards from Astra Zeneca, Boehringer-Ingelheim, Echosens, Eli Lilly, Madrigal, MSD, Novo Nordisk, Target RWE, and and investigator-initiated research support from Boehringer-Ingelheim, Nutricia/Danone, and Sanofi-Aventis. The other authors declare that they have no competing interests. **Data and materials availability:** All data needed to evaluate the conclusions of the paper are present in the paper and/or the Supplementary Materials.

Submitted 22 July 2024
Accepted 26 November 2024
Published 1 January 2025
10.1126/sciadv.adr8849